University of Thessaly

Department of Mechanical Engineering

Dual Kalman Filtering algorithm for joint input state estimation using output-only vibration measurements

Systems Dynamics Laboratory

Diploma Thesis of

Georgios D. Pasparakis

Thesis Supervisor: **Dr. Costas Papadimitriou**

Submitted in partial fulfillment of the requirements for the Mechanical Engineering Diploma from University of Thessaly.

Volos, July 2018

Thesis Committee

Dr. Costas Papadimitriou

Professor of Structural Dynamics, Department of Mechanical Engineering, University of Thessaly.

Dr. Spyros A. Karamanos

Professor of Numerical Methods - Finite Elements - Structural Mechanics, Department of Mechanical Engineering, University of Thessaly.

Dr. Nikolaos Aravas

Professor of Computational Mechanics, Department of Mechanical Engineering, University of Thessaly.

Acknowledgments

For the development of my diploma thesis I would like to express my gratitude to my supervisor Prof. Costas Papadimitriou for his invaluable support and guidance throughout my learning process.

I would also like to thank my friends and family for their presence during the year of my studies.

This thesis is dedicated to my mother and my father

Summary

Modern day structures are subject to unknown input forces during their operational life span leading to fatigue damage accumulation over time. The current diploma thesis utilizes a dual Kalman filtering methodology in a stochastic framework in order to identify these input forces applied on a spring mass like chain model, equivalent to a simplified linear model of a structure. The extent of estimating accuracy of the proposed scheme is investigated in a variety of cases for multiple forces non or collocated. It is shown that by obtaining a number of response measurements at certain locations i.e. degrees of freedom of the system, strain and consequently stress time histories can by calculated. An estimate of the fatigue damage and subsequently an accurate lifetime prognosis can be obtained. The effect of the measurement location in relation to load application is examined and tuning methods are implemented in order to obtain more accurate response and input estimates. Lastly, the algorithm is tested on a substructure model of a linear system in order to evaluate the efficiency of the algorithm in terms of response, strain and stress time histories and subsequently fatigue damage.

Table of contents

Introduction

Vibration induced by uncertain loading is a common case in structures that operate in dynamic environments such as wind turbines, bridges and buildings etc. while technological advancement causes the emergence of structures of ever growing complexity. It is therefore imperative the development of accurate modeling tools and prediction methodologies in order to insure a safe operational environment for these structures as well as for the people surrounding them. This task lies in the field of structural health monitoring and extensive research is under way in that direction.

The subject of this diploma thesis tackles the problem of jointly estimating the state and unknown input in a linear model via the implementation of a Dual Kalman filtering algorithm for a number of applied inputs. Dealing with structural systems, the states of the system are displacements and velocities of the response of the system at some points, namely degrees of freedom (DOF) on the structure. The kinematic relations between these parameters enter the dynamic model of the system and coupled with a number of partially observed states i.e. measurements, produce estimates for all the states of the system as well as for the input forces that are applied. The filter used in this case is the one proposed be Eftekhar Azam, E. Chatzi and C. Papadimitriou [1] for a number of acceleration measurements and C. Papadimitriou and C. P. Fritzen [2] and focuses on linear systems. Dealing with non – linear systems other algorithms are studied such as the unscented Kalman filter and the particle filter [3] [4].

An important aspect of the estimating efficiency of the proposed algorithm is conditioned on the appropriate selection of the Covariance matrices that consist the statistical knowledge of the excitation at hand. Such techniques for tuning the appropriate Covariance values have been studied from S. Gillijns, B. De Moor [5]and S.Bittanti, S. M. Savaresi [6] ,[7] in order to mitigate the drift effects arising in parameter estimates and are implemented throughout this thesis.

The process of obtaining accurate displacement time histories all over the structure, enables the formulation of the displacement field an thus the calculation of the strain and stress time histories. Making use of existing stress cycle counting methods such as Rainflow counting methods and implementing them in linear damage accumulation laws like the Palmgren-Miner [8], [9] and experimental S-N curves, furnished estimates on the fatigue

damage on all locations of the structure can be produced as studied from C. Papadimitriou, C. P. Fritzen [10].

Lastly, the proposed case and methodology formed in this thesis is implemented in a sub-structured system of an original shear type building formulation as an equivalent to earthquake base excitation.

Chapter 1

Dual Kalman Filtering algorithm for joint input state estimation in mass-spring chain like models

1.1 Mathematical Formulation of discrete state space equations

The governing equation of a linear structural dynamics problem is typically formulated using the following continuous time second order differential equation:

$$\boldsymbol{M\ddot{u}}(t)\boldsymbol{+ C\dot{u}}(t) + \boldsymbol{Ku}(t) = \boldsymbol{f}(t) = \boldsymbol{S_p p}(t) \quad (1)$$

where $\boldsymbol{u}(t)$ is a matrix $\in R^{nxn}$ stands for the displacement, **K, M** and **C** $\in R^{nxn}$ are symmetric matrices that stand for stiffness, damping and mass respectively. The notation n stands for the degrees of freedom of the system and vector $\boldsymbol{f}(t) \in R^n$ is defined as the excitation force. The excitation force will be herein presented as a superposition of time histories $\boldsymbol{p}(t) \in R^{n_p}$ that are influencing certain degrees of freedom of the system according to the respective influence matrix $\boldsymbol{S_p} \in R^{nxn_p}$.

The problem is subsequently formulated in state space form by introducing the state vector:

$$\boldsymbol{x}(t) = \begin{bmatrix} \boldsymbol{u}(t) \\ \dot{\boldsymbol{u}}(t) \end{bmatrix} \quad (2)$$

where $\boldsymbol{x}(t) \epsilon R^{2nx1}$ by doing so Eq. (1) can be rewritten to constitute the process equation:

$$\dot{\boldsymbol{x}}(\boldsymbol{t}) = \boldsymbol{A_c x}(t) + \boldsymbol{B_c p}(t) \quad (3)$$

where $\boldsymbol{A_c} \epsilon R^{2nx2n}$ and $\boldsymbol{B_c} \epsilon R^{2nx2}$ are the following matrices :

$$\boldsymbol{A_c} = \begin{bmatrix} \boldsymbol{0} & \boldsymbol{I} \\ \boldsymbol{-M^{-1}K} & \boldsymbol{-M^{-1}C} \end{bmatrix}$$

$$\boldsymbol{B_c} = \begin{bmatrix} \boldsymbol{0} \\ \boldsymbol{M^{-1}S_p} \end{bmatrix}$$

Regarding the measurement equation a general case of a vector $\boldsymbol{d}(t) \epsilon R^{n_o x1}$ containing displacement, velocity and acceleration measurements is considered.

$$\boldsymbol{d}(t) = \begin{bmatrix} \boldsymbol{S_d} & \boldsymbol{0} & \boldsymbol{0} \\ \boldsymbol{0} & \boldsymbol{S_v} & \boldsymbol{0} \\ \boldsymbol{0} & \boldsymbol{0} & \boldsymbol{S_a} \end{bmatrix} \begin{bmatrix} \boldsymbol{u}(t) \\ \dot{\boldsymbol{u}}(t) \\ \ddot{\boldsymbol{u}}(t) \end{bmatrix}$$

Where $\boldsymbol{S_d}, \boldsymbol{S_v}, \boldsymbol{S_a} \in R^{n_d x\, n}$ are the selection matrices of appropriate dimension for the displacements, velocities and accelerations respectively. The term n_d stands for the number of observations of displacements, velocities and accelerations for each of component. These matrices identify which degree of freedom measurements are taken from and in this thesis mainly accelerations and displacement measurements are used.

The equivalent state space form of the measurement vector can be given by

$$\boldsymbol{d}(t) = \boldsymbol{G_c}\, \boldsymbol{x}(t) + \boldsymbol{J_c}\boldsymbol{p}(t) \tag{4}$$

where the matrices $\boldsymbol{G_c} \in R^{n_d x\, 2n}$ and $\boldsymbol{J_c} \in R^{n_d x\, 2}$ are

$$\boldsymbol{G_c} = \begin{bmatrix} \boldsymbol{S_d} & \boldsymbol{0} \\ \boldsymbol{0} & \boldsymbol{S_v} \\ -\boldsymbol{S_a M^{-1} K} & -\boldsymbol{S_a M^{-1} C} \end{bmatrix}$$

$$\boldsymbol{J_c} = \begin{bmatrix} \boldsymbol{0} \\ \boldsymbol{0} \\ \boldsymbol{S_a M^{-1} S_p} \end{bmatrix}$$

In practice though, the state vector of Eq. (1) can become relatively large when dealing with fine resolution finite element models (FE). Despite that the dynamics of the system could effectively be captured by a significantly smaller number of modes. To suppress the computational costs associated with the large FE models, Eq. (1) is projected in the subspace spanned by a limited number of the undamped eigenmodes of the system. The corresponding eigenvalue problem of Eq. (1) is the following:

$$\boldsymbol{K\Phi} = \boldsymbol{M\Phi\Omega^2} \tag{5}$$

where $\boldsymbol{\Phi} \in R^{\boldsymbol{nxm}}$ are the eigenvectors of the modes of the system and have to satisfy the orthogonality conditions $\boldsymbol{\Phi^T M\Phi} = \boldsymbol{I}$, $\boldsymbol{\Phi^T K\Phi} = \boldsymbol{\Omega^2}$, $\boldsymbol{\Phi^T C\Phi} = \boldsymbol{\Gamma}$ where $\boldsymbol{\Omega} \in R^{\boldsymbol{nxn}}$ is a diagonal matrix containing the values of the eigenfrequencies of the system. $\boldsymbol{\Gamma} \in R^{nxn}$ is the diagonal damping matrix with $2\xi_i$ diagonal elements and ξ_i stand for the relevant damping ratios of each mode.

In order to project the coordinate system into the subspace spanned by the undamped eigenmodes of the system of Eq. (1) the following coordinate system transform is introduced:

$$\boldsymbol{u}(t) = \boldsymbol{\Phi}\,\boldsymbol{z}(t) \tag{6}$$

and Eq.1 becomes:

$$\boldsymbol{\Phi}^{\boldsymbol{T}}\boldsymbol{M}\boldsymbol{\Phi}\ddot{\boldsymbol{z}}(t) + \boldsymbol{\Phi}^{\boldsymbol{T}}\boldsymbol{C}\boldsymbol{\Phi}\dot{\boldsymbol{z}}(t) + \boldsymbol{\Phi}^{\boldsymbol{T}}\boldsymbol{K}\boldsymbol{\Phi}\boldsymbol{z}(t) = \boldsymbol{\Phi}^{\boldsymbol{T}}\boldsymbol{S}_{\boldsymbol{p}}\boldsymbol{p}(t)$$

and based on the orthogonality conditions introduced previously Eq. (1) takes the following form:

$$\ddot{\boldsymbol{z}}(t) + \boldsymbol{\Gamma}\dot{\boldsymbol{z}}(t) + \boldsymbol{\Omega}^{\boldsymbol{2}}\boldsymbol{z}(t) = \boldsymbol{\Phi}^{\boldsymbol{T}}\boldsymbol{S}_{\boldsymbol{p}}\boldsymbol{p}(t) \tag{7}$$

In case of a reduced order state space model a truncated eigenvector space can be substituted in Eq.(7) and a modal analysis can take place as follows:

$$\boldsymbol{x}(t) = \begin{bmatrix} \boldsymbol{\Phi}_{\boldsymbol{\Gamma}} & \boldsymbol{0} \\ \boldsymbol{0} & \boldsymbol{\Phi}_{\boldsymbol{\Gamma}} \end{bmatrix} \boldsymbol{\zeta}(t)$$

where $\boldsymbol{\zeta}(t) \in R^{2m}$ is the truncated modal vector corresponding to m modes that are chosen to participate in the response. In order to obtrain a modal state space representation of the original problem the modal state vector is introduced:

$$\boldsymbol{\zeta}(t) = \begin{bmatrix} \boldsymbol{z}(t) \\ \dot{\boldsymbol{z}}(t) \end{bmatrix}$$

Consequently, the continuous state space equation takes the following form:

$$\dot{\boldsymbol{\zeta}}(t) = \boldsymbol{A}_{\boldsymbol{c}}\boldsymbol{\zeta}(t) + \boldsymbol{B}_{\boldsymbol{c}}\boldsymbol{p}(t) \tag{8}$$

$$\boldsymbol{d}(t) = \boldsymbol{G}_{\boldsymbol{c}}\,\boldsymbol{\zeta}(t) + \boldsymbol{J}_{\boldsymbol{c}}\boldsymbol{p}(t) \tag{9}$$

where the appropriate matrices are:

$$\boldsymbol{A}_{\boldsymbol{c}} = \begin{bmatrix} \boldsymbol{0} & \boldsymbol{I} \\ \boldsymbol{\Omega}^{\boldsymbol{2}} & -\boldsymbol{\Gamma} \end{bmatrix}$$

$$\boldsymbol{B}_{\boldsymbol{c}} = \begin{bmatrix} \boldsymbol{0} \\ \boldsymbol{\Phi}_{\boldsymbol{\Gamma}}{}^{\boldsymbol{T}}\boldsymbol{S}_{\boldsymbol{p}} \end{bmatrix}$$

$$\boldsymbol{G_c} = \begin{bmatrix} \boldsymbol{S_d \Phi_\Gamma} & \boldsymbol{0} \\ \boldsymbol{0} & \boldsymbol{S_v \Phi_\Gamma} \\ \boldsymbol{-S_a \Phi_\Gamma \Omega^2} & \boldsymbol{-S_a M^{-1} C} \end{bmatrix}$$

$$\boldsymbol{J_c} = \begin{bmatrix} \boldsymbol{0} \\ \boldsymbol{0} \\ \boldsymbol{S_a \Phi_\Gamma \Phi_\Gamma{}^T S_p} \end{bmatrix}$$

In order to discretized Eqs.(8) and (9), the sampling rate is denoted by $1/\Delta t$ and the discrete state space equation obtains the following form:

$$\boldsymbol{\zeta_{\kappa+1}} = \boldsymbol{A\zeta_\kappa + B_c p_k} \quad (10)$$

$$\boldsymbol{d_k} = \boldsymbol{G\,\zeta + J_c p_k} \quad (11)$$

where $\boldsymbol{A = e^{A_c \Delta t}}$, $\boldsymbol{B = [A - I] A_c^{-1} B_c}$, $\boldsymbol{G = G_c}$ and $\boldsymbol{J = J_c}$.

1.2 Dual Kalman filter for joint input state estimation

In this section a dual implementation of the Kalman filter for a joint – input state estimation attempt. The state space Eqs. (10) and (11) can be formulated into state process form under the following assumption:

$$\boldsymbol{\zeta_{k+1}} = \boldsymbol{A\zeta_k} + \boldsymbol{Bp_k} + \boldsymbol{v_k^\zeta} \quad (12)$$

$$\boldsymbol{d_k} = \boldsymbol{G\zeta_k + Jp_k + w_k} \quad (13)$$

where v_k^ζ is the process noise assumed, zero-mean white with Covariance $\boldsymbol{Q^\zeta}$ and w_k is the zero mean, white, measurement noise with covariance $\boldsymbol{R}$. The two processes are mutually uncorrelated. Also, the unknown input is calibrated through the fictitious process equation :

$$\boldsymbol{p_{k+1}} = \boldsymbol{p_k} + \boldsymbol{v_k^p} \quad (14)$$

where v_k^p is a zero mean white Gaussian process with it's associated covariance matrix Q^p.

Recombining Eqs. (13) and (14) a new state process equation can be obtained:

$$\boldsymbol{p_{k+1}} = \boldsymbol{p_k} + \boldsymbol{v_k^p} \quad (15)$$

$$\boldsymbol{d_k = G\zeta_k + Jp_k + w_k} \quad (16)$$

In that respect, the sought for parameter of estimation is now the fictitious force process $\boldsymbol{p_k}$ based on observations $\boldsymbol{d_k}$ and now $\boldsymbol{\zeta_k}$ plays the role of the input of the system.

Thus a two stage scheme can be proposed with the Kalman Gain pertaining in both stages. The first part of the algorithm is constituted by the estimation of the input and the second by the updating of the state based on the updated input.

Specifically, the algorithm is initiated by evaluating the estimates at time = 0 for the state and the input. The same applies for the initial values of their corresponding Covariances:

$$\widehat{\boldsymbol{\zeta_0}} = \mathrm{E}[\boldsymbol{\zeta_0}]$$

$$\widehat{\mathbf{p_0}} = \mathrm{E}[\mathbf{p_0}]$$

$$P_0 = E[(\boldsymbol{\zeta_0} - \widehat{\boldsymbol{\zeta_0}})]$$

$$P_0^p = E[(\mathbf{p_0} - \widehat{\mathbf{p_0}})(\mathbf{p_0} - \widehat{\mathbf{p_0}})^{\mathrm{T}}]$$

The successive structure of the DKF algorithm starts with the evolution of the input and the prediction of it's corresponding Covariance:

$$\boldsymbol{p_k^-} = \boldsymbol{p_{k-1}}$$

$$\boldsymbol{P_k^{P-}} = \boldsymbol{P_{k-1}^P} + \boldsymbol{Q^p}$$

Next, follows the calculation of the Kalman gain for the input:

$$\boldsymbol{G_k^P} = \boldsymbol{P_k^{P-} J^T (J P_k^{P-} J^T} + \boldsymbol{R})^{-1}$$

The predictions are then improved based on the latest observations:

$$\widehat{\boldsymbol{p_k}} = \boldsymbol{p_k^-} + \boldsymbol{G_k^p}(\boldsymbol{d_k} - \boldsymbol{G}\hat{\boldsymbol{\zeta}}_{\boldsymbol{k-1}} - \boldsymbol{J p_k^-})$$

$$\boldsymbol{P_k^P} = \boldsymbol{P_k^{P-}} - \boldsymbol{G_k^p J P_k^{p-}}$$

Next, the state and its Covariance are predicted:

$$\boldsymbol{\zeta_\kappa^-} = \boldsymbol{A}\hat{\boldsymbol{\zeta}}_{\boldsymbol{k-1}} + \boldsymbol{B}\widehat{\boldsymbol{p}}_{\boldsymbol{k}}$$

$$\boldsymbol{P_k^-} = \boldsymbol{A P_{k-1} A^T} + \boldsymbol{Q^\zeta}$$

Lastly, the Kalman Gain for the state is calculated and the predictions are improved in the same fashion as in the previous stage of the input:

$$\boldsymbol{G_k^\zeta} = \boldsymbol{P_k^- G^T (G P_k^- G^T} + \boldsymbol{R})^{-1}$$

$$\hat{\boldsymbol{\zeta}}_{\boldsymbol{k}} = \boldsymbol{\zeta}_{\boldsymbol{\kappa}}^{-} + \boldsymbol{G}_{\boldsymbol{k}}^{\boldsymbol{\zeta}}(\boldsymbol{d}_{\boldsymbol{k}} - \boldsymbol{G}\boldsymbol{\zeta}_{\boldsymbol{\kappa}}^{-} - \boldsymbol{J}\hat{\boldsymbol{p}}_{\boldsymbol{k}})$$

$$P_k = P_k^{-} - \boldsymbol{G}_{\boldsymbol{k}}^{\boldsymbol{\zeta}}\boldsymbol{G}\boldsymbol{P}_{\boldsymbol{k}}^{-}$$

Chapter 2

Algorithm Description

2.1 Methodology

The methodology followed in this diploma thesis can be captured in the following simplified flow diagram. At first, model matrices are formed i.e., **K, M** and **C** depending on the system properties specified or can either be loaded from data obtained by a finite element analysis. As stated in the mathematical formulation, two different approaches of estimation can be followed with one being through the calculation of the matrices **K, M** and **C** and the other by solving the eigenvalue problem.

These are then can be rewritten to have a state space representation in time continuous form and then are discretized in time via a zero order hold (ZOH) assumption, which assumes a constant inter – sample behavior of the input. In this case the sampling frequency is 100 Hz. The measurements are thought to be lasting $25\ secs$ and as a result the signal composes of 2500 discrete time instances

The simulated location of the load has to be subsequently specified and a generated response (output) of the system is obtained considering known accelerations or displacements according to the observations that are available for the system each time. These measurements are thought to be noise contaminated with a Gaussian white noise process with zero mean and Covariance R.

The same state space formulation is used for the implementation of the Dual Kalman Filter (DKF) according to the location of the force that is considered. It is worth noting that for the DKF to produce reasonable results, the number of observations should be equal or greater than the number of applied loads in case of non-collocated inputs. Moreover, it is considered that at points of measurement loads are being applied. Inputs are produced through a Gaussian White process with zero mean and variance of value of 1.

State and input are computed into process equation forms and as such, they have two associated noise Covariance matrices Q^x , Q^p. A prior knowledge of the initial values of these Covariances is a presupposition for the DKF procedure to produce results.

These Covariances together with measurement Covariance R are of essential importance to the estimation accuracy of the sought for parameter and serve as a tuning knob for the estimation task at hand. Their importance will be illustrated later in this thesis.

Generally, state Covariance Q^x indicates the confidence put in the model. The lower the value of Q^x is, the more accurate the model is considered to be. In the same manner the Covariance value R reveals the confidence put into the measurement and the lower its value, the tighter the fit of the estimation to the data should be.

After the implementation of the DKF procedure the estimated data are plotted in cross comparison to the simulated ones in order to test the estimating accuracy of the algorithm.

The prominent goal is to be able to estimate all the partially observed states of the system as well as the input through a number of acceleration measurements and/or displacements. The accurate estimation of the displacements of the system can serve the purpose of the estimation of the fatigue of the structure and help calculate its remaining time life.

Also great emphasis is given to the estimation of the input forces whose locations are not always known or are at certain cases collocated.

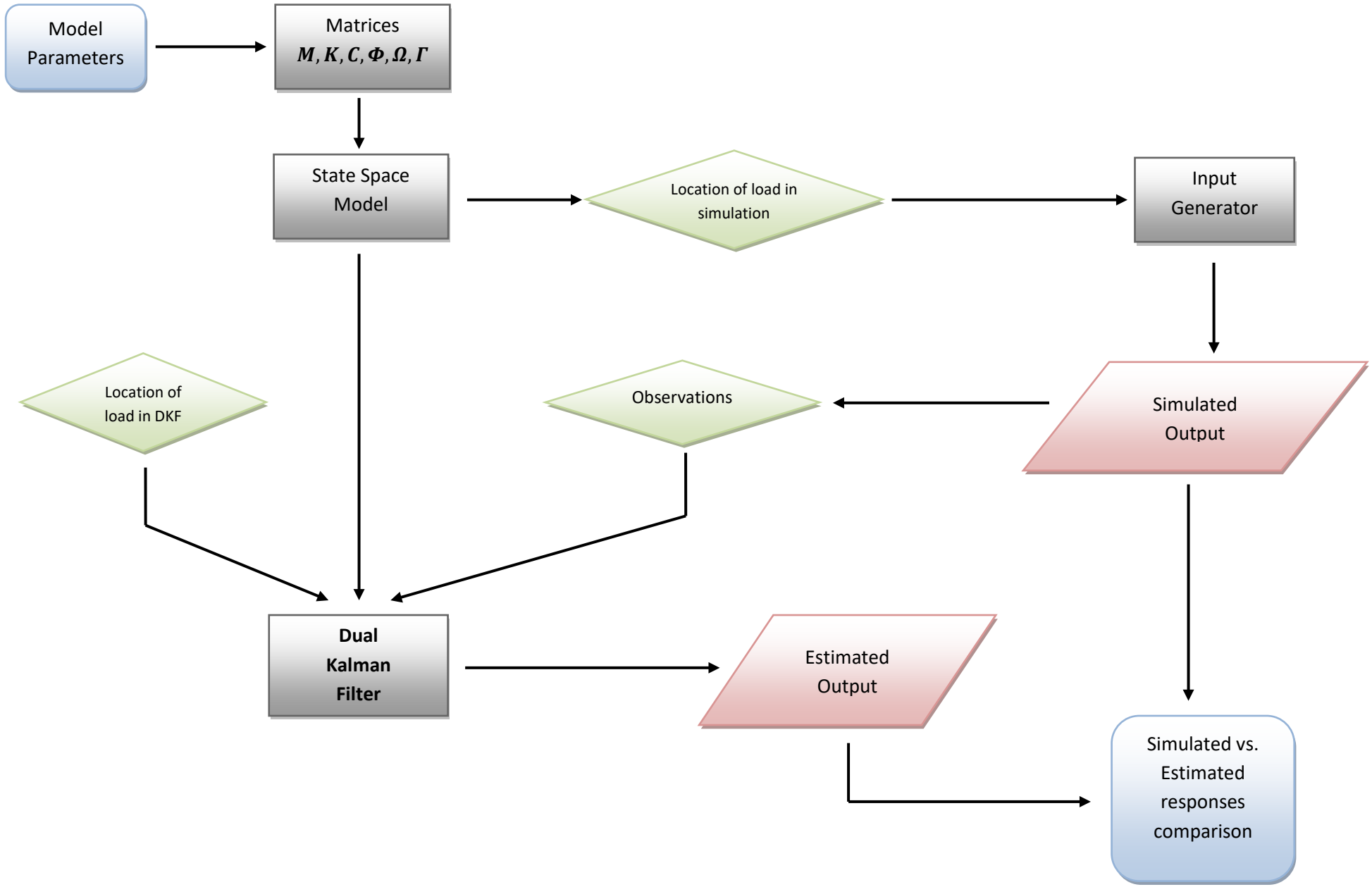

Fig. 2.1 : Schematic representation of the Dual Kalman filtering algorithm.

Chapter 3

Application to spring-mass model

3. 1 Model specification

The model which will be herein considered will be one of spring mass chain. Specifically, it is considered to have the following properties:

$Ndof = 10$ are the degrees of freedom of the system.
$m = 0.35\ kg$ is each mass of the respecting degree of freedom.
$K = 600\ N/m$ is the stiffness of each spring.
$\zeta = 0.05$ is the damping ratio of each mode.

The system is supposed to model the properties of a 10 degree of freedom spring-mass chain like system where each mass represents the mass of the DOF, the spring stiffness represents the inter mass stiffness with a respective damping ratio of 5% at each mode.
The eigenvalues of each node of the system i.e. the natural frequencies are presented in the following table.

Vibration mode index	Natural frequency (Hz)
1	1,0251
2	3,0524
3	5,0115
4	6,8587
5	8,5527
6	10,056
7	11,334
8	12,359
9	13,109
10	13,564

Table 3.1: Vibrational eigenfrequencies of the system

3.2 Simulated examples

3.2.1 Case no.1 -Two collocated Inputs at a known location

In the first case, two inputs are being asked both at three degrees of freedom of the system and one measurement of acceleration is being obtained. The number of inputs is considered to be known as well as the location of their application.

Simulation parameters	
Number of loads = 2	DOF
Load #1	3rd
Load #2	3rd

Table3.1: Simulation Parameters for case no.1

DKF parameters	
Number of observations = 1	DOF
Observation of accelerations	3rd

Table3.2: DKF Parameters for case no.1

The initial values of the Covariance of the diagonal components of the state Covariance matrix are set at $Q^x = 10^{-20}$ whereas the corresponding values of the Input Covariance are set at $Q^p = 10^{-1}$. Also, the initial values for the measurement covariance R are set to 1% of the maximum measured acceleration.

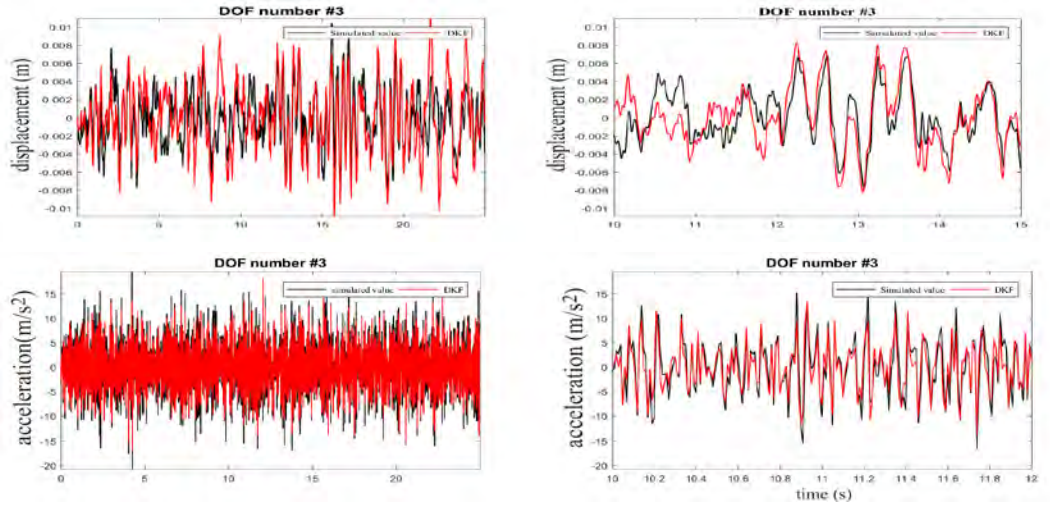

Figure 3.1: Response time histories for the observed 3rd degree of freedom for case no.1

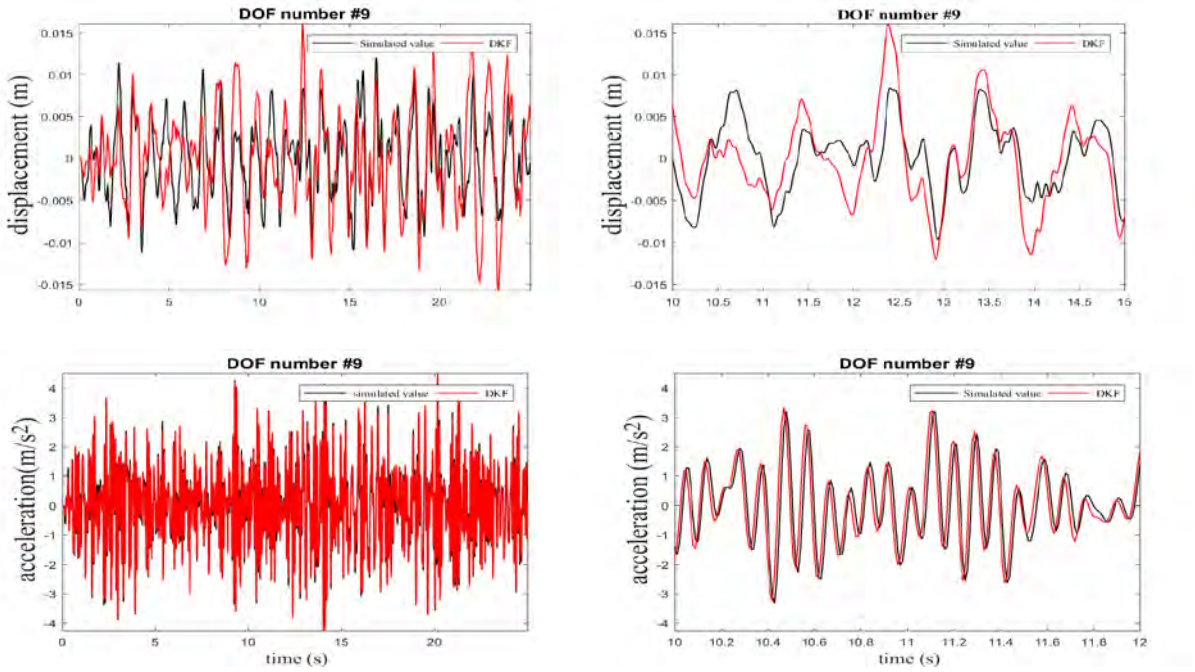

Figure 3.2: Response time histories for the unobserved 9th degree of freedom for case no.1

By examining the results of the response time histories for the observed 3rd and the unobserved 9th degree of freedom it is evident that despite only one acceleration measurement, the DKF algorithm produces a good estimate regarding the accelerations of the system both observed and unobserved. On the other hand, significant drifts tend to appear in terms of displacements between the simulated and DKF values.

3.2.2 Tuning the measurement Covariance matrix

In order to mitigate the lack of estimation accuracy the values of the values of noise Covariance R are reexamined. A methodology is proposed for a more accurate evaluation of these values that constitute à priori knowledge for the system.

In that respect the standard deviation of each acceleration measurement is introduced:

$$std_k = \sqrt{\frac{\sum_{i=1}^{Nt} d_i}{Nt}}$$

Where Nt is the number of time instances the signal is composed of and d_i are the respective measurements in the ith degree of freedom of the system. Furthermore, it is considered that the standard deviation is approximately 1% of the measurement of each peak acceleration and thus $s_k = \frac{std_k}{100}$, where k corresponds to the reciprocal number of measurement.

Concluding, the values of the noise Covariance R will have the following form $\boldsymbol{R = s^2 * I}$ where $\boldsymbol{I}$ is the identity matrix with the appropriate dimensions conditioned on the number of measurements available.

In this case, $R_1 = \mathbf{0.003}$ whereas the previous value was $R_2 = \mathbf{0.1951}$

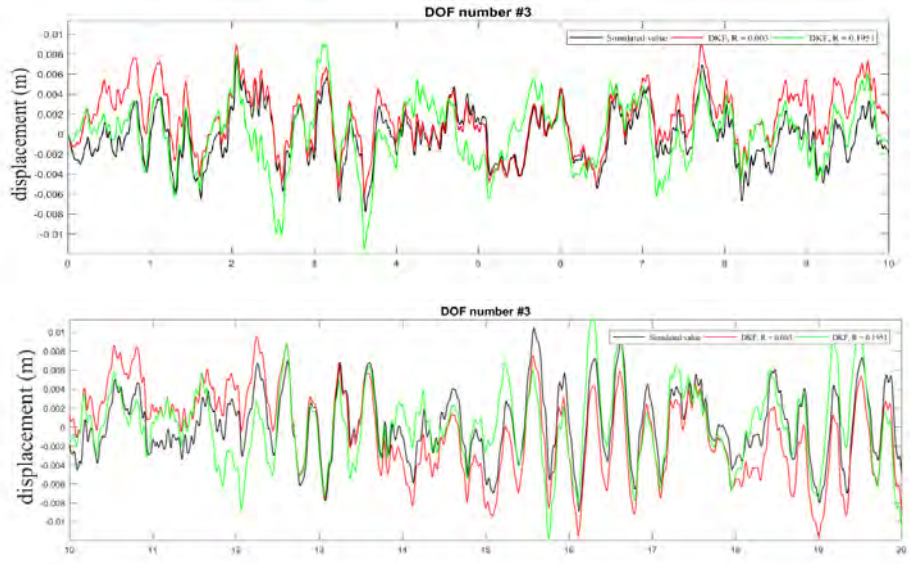

Fig. 3.3: Displacement time history of the 3rd degree of freedom fo case no.1

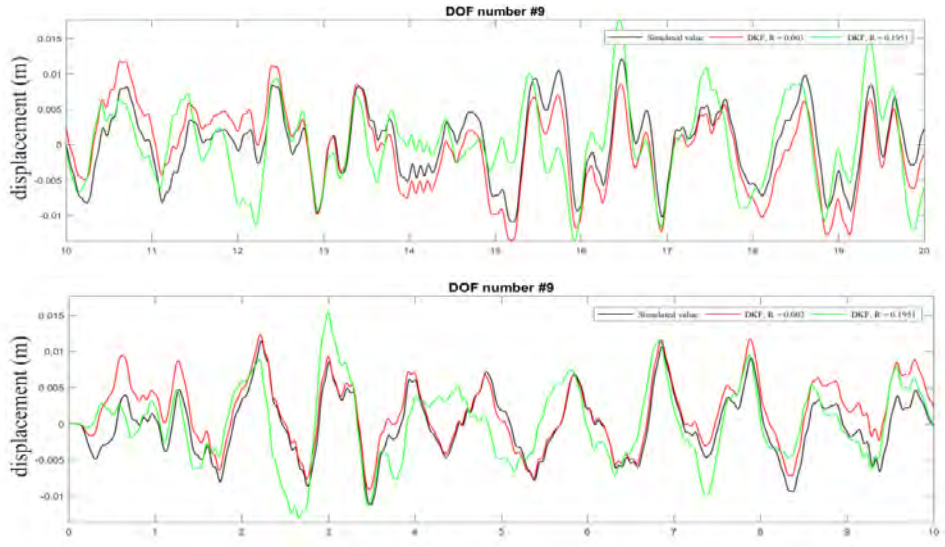

Fig. 3.3: Displacement time history of the 9th degree of freedom for case no.1

The same methodology can be used without loss of generality for displacement measurements. The updated estimates in cross comparison to the ones before the tuning are presented in Fig 3.3 and Fig 3.4.

Examining the results presented in these figures, it becomes evident that the updated values of the noise Covariance do not achieve to produce completely furnished results mainly because drifts appear with periodicity within the signal. Notwithstanding, the updated estimates tend to follow the path of the simulated outputs in a more accurate manner even when drifts appear. More noticeable drifts occur in the 3rd degree of freedom where the loads are being applied. This tendency is less intense in the 9th degree of freedom where a noticeably better estimate is produced compared to the previous one.

Regarding the accuracy of the estimate of the Inputs it comes with significant drifts as illustrated in Fig. 3.5:

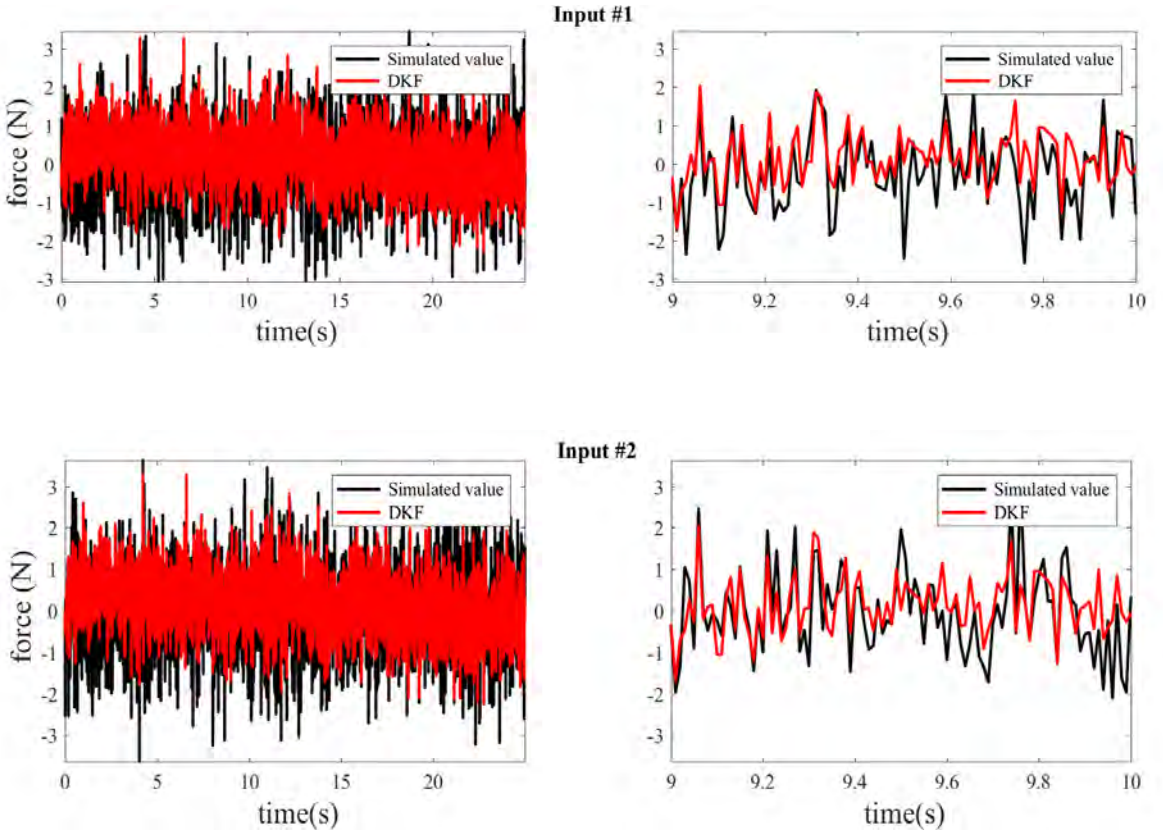

Figure 3.5: Displacement time histories for the unobserved 9^{h} degree of freedom for t = 0-10 sec and 10 -25 sec for different measurement Covariances

The main reason for this discrepancy is the fact that the number of measurements is less than the number of applied loads. However, the fact that the loads are applied at the same degree of freedom which is observed enables DKF to produce a rough estimate on the Input forces.

3.2.3 Case no.2 -2 non-collocated Inputs at partially measured locations

In the second case, two different loads are applied at four different degrees of freedom of the system (DOF). The applied loads are not collocated and acceleration and displacement measurements are taken into account, only from two of the four degrees of freedom in which the loads are applied.

Simulation parameters	
Number of loads =2	DOF
Load #1	3^{rd} , 5^{th}
Load #2	7^{th}, 10^{th}

Table 3.3 : Simulation Parameters for case no.2

DKF parameters	
Number of observations = 2	DOF
Observation of accelerations	5^{th} , 7^{th}

Table 3.4 DKF Parameters for case no.2

The initial values of the Covariance of the diagonal components of the state Covariance matrix are set at $Q^x = 10^{-30}$ whereas the corresponding values of the Input Covariance are set at $Q^p = 10^{-1}$. Regarding the values of the noise Covariance R the values are set in the same methodology as proposed previously.

At this stage two separate individual sub -cases are examined, regarding the knowledge of the location of the applied loads.

In the first sub - case it is considered that the exact distribution of the loads is known and therefore it is taken into account that first and second load are acting upon the 3^{rd}, 5^{th} and 7^{th} and 10^{th} degree of freedom respectively.

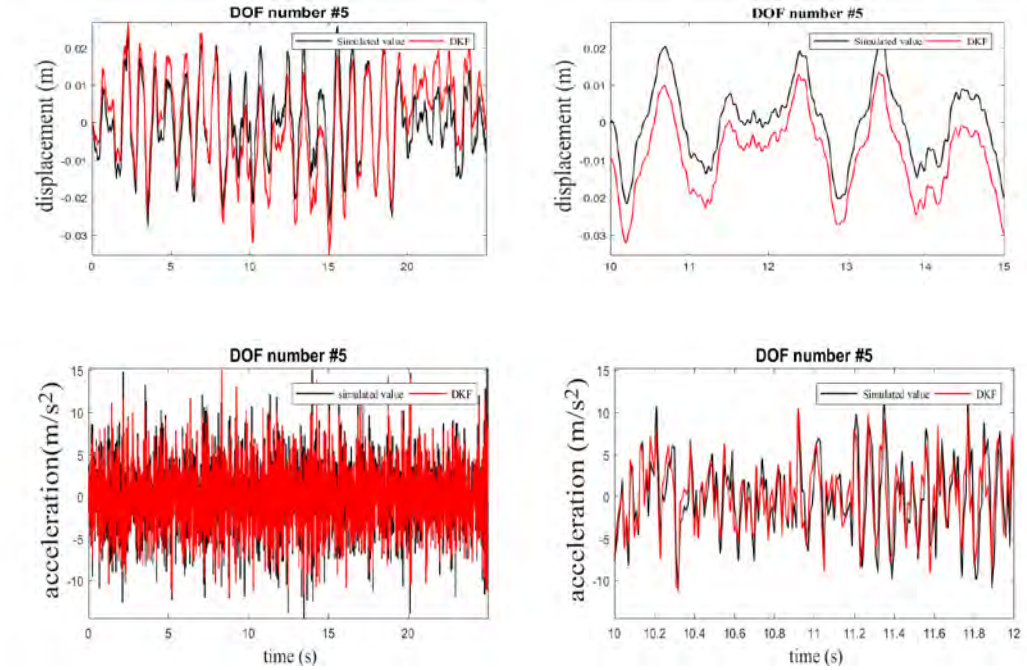

Figure 3.6 : Response time histories for the observed 5th degree of freedom for case no.2

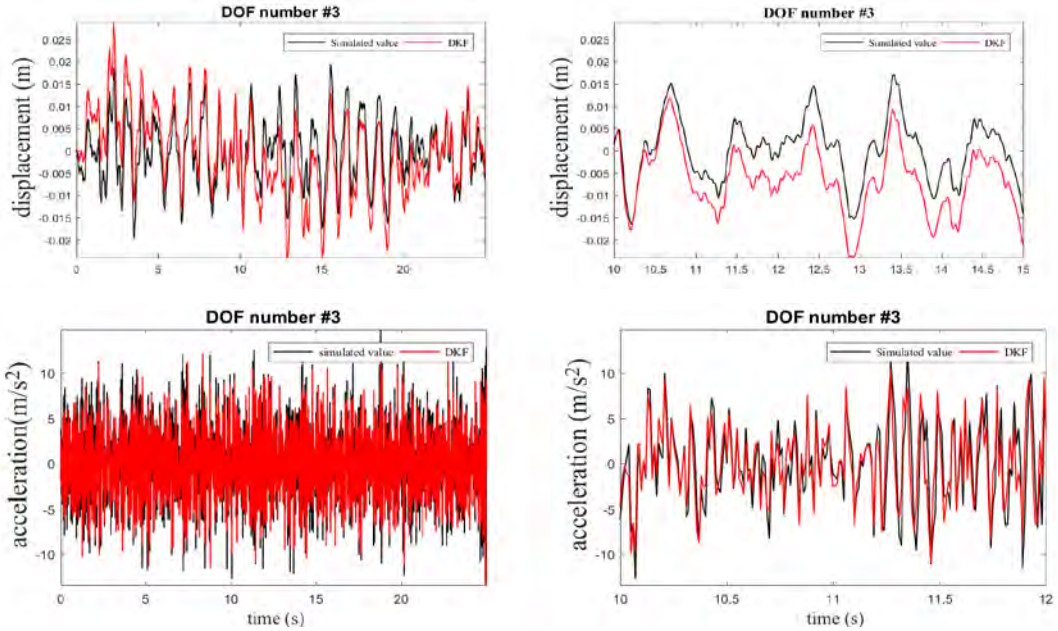

Figure3.7: Response time histories for the unobserved 3rd degree of freedom where load is applied for case no.2

By close examination of the responses of the 5th and 3rd degree of freedom DKF once again proves as a good estimating tool in terms of acceleration estimates. Despite that drifts seem to appear in displacement estimates in all degrees of freedom of the system even at points where no load is applied as shown for instance in Fig. 3.8

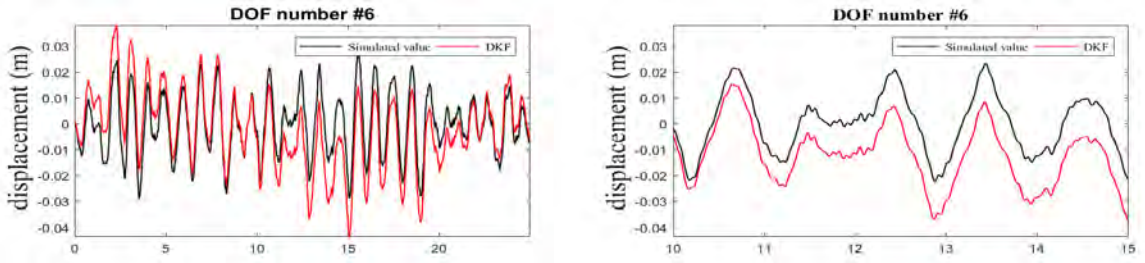

Figure3.8: Response time histories for the unobserved 3rd degree of freedom where no load is applied for case no.2

As far as the input estimation is concerned, no drifts seem to appear and the inputs are approximated at high level of accuracy as shown in Fig. 3.9

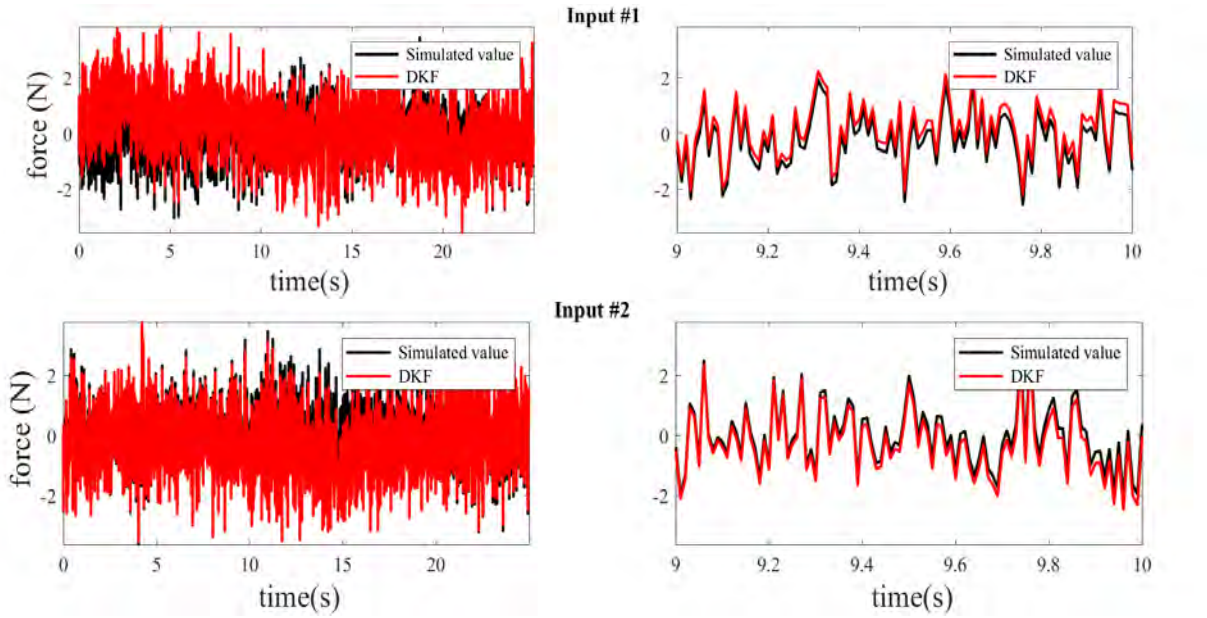

Figure 3.9 : Force time histories estimates for t = 0 – 25 sec and t =9-10sec

The ability of DKF to produce good results regarding the input loads is in partly conditioned on the knowledge of the location of the loads. Despite not obtaining measurements at points where the forces are acting upon, the knowledge of their application proves to be sufficient for an accurate estimation of the input forces.

Considering the second sub - case it is considered that the exact distribution of the loads is partially known and thus the first and second load are thought to be acting now only on the 5th and 7th degrees of freedom i.e. only on the points where measures are being obtained from which the most usual case when trying to estimate unknown input forces.

In this case, the lack of information deteriorates the estimates in regard of accelerations where as the ones of displacements are mildly affected. This tendency is especially high for the unobserved points of load application. Moreover, the estimates on the unknown input forces seem to be presenting noticeable drifts. The indicative results are presented in Fig. 3.10 and 3.11

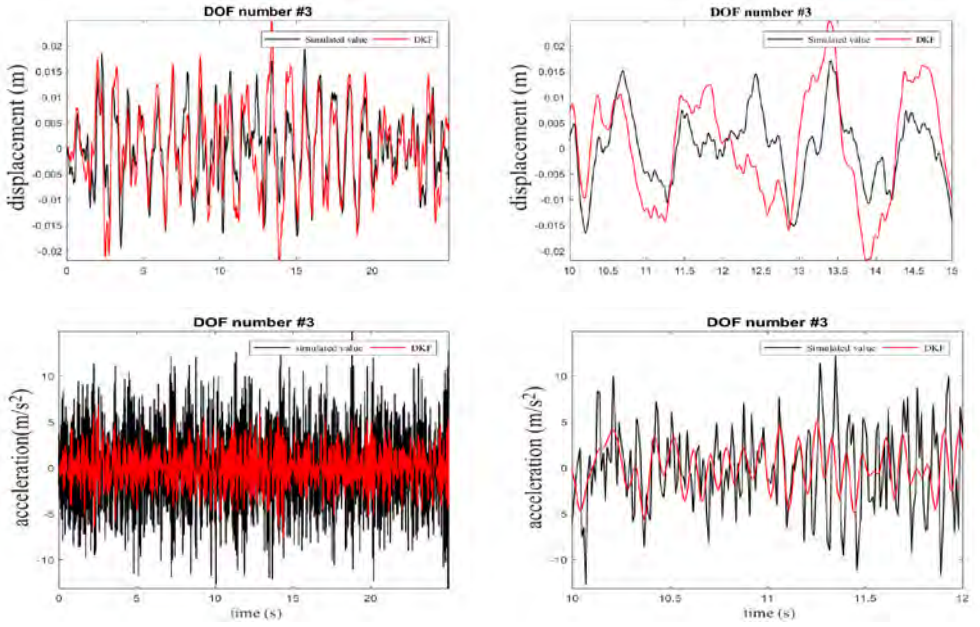

Figure 3.10: Response time histories for the unobserved 3rd degree of freedom where load is applied

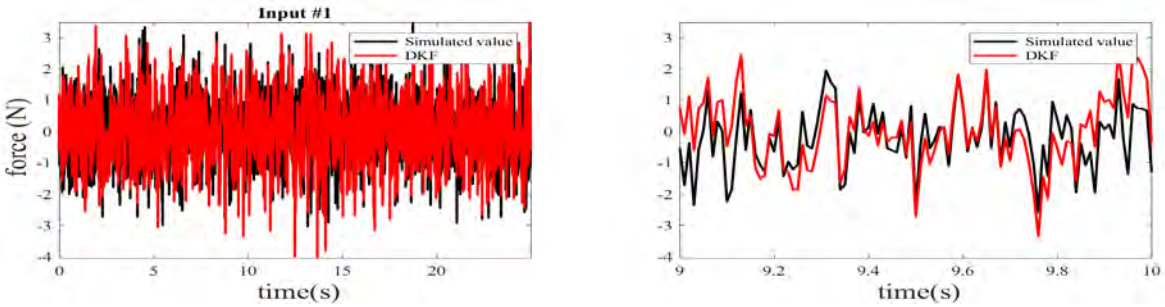

Figure 3.11: Force time history estimate for t = 0 – 25 sec of the 1st input for case no.2b

3.2.4 Effects of displacement measurements

In this part, the effect of the displacement measurements are being examined in order to examine whether obtaining such measurements contributes to the elimination of the drifts that seem to appear. In this direction, the case no. 2a is being revisited but this time obtaining two displacement measurements on the 5th and 7th degree of freedom where also the acceleration measurements are obtained from.

The results are presented in Fig. 3.12

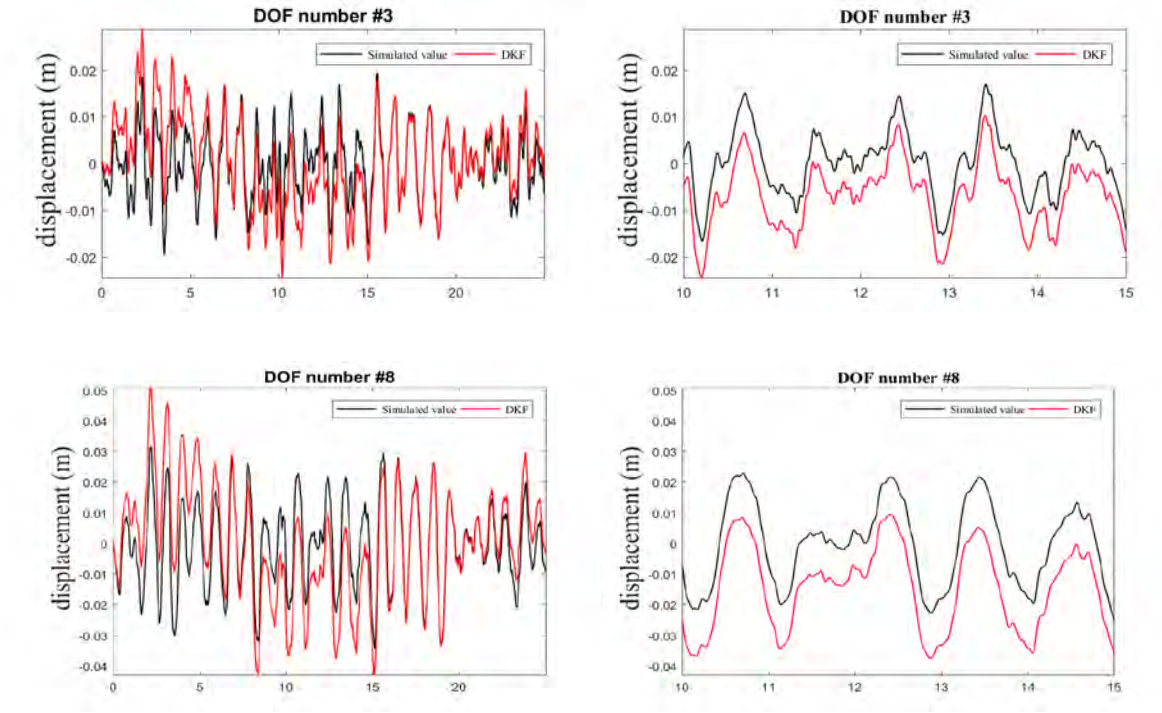

Fig 3.12: Displacement time histories for 3rd and 8th degree of freedom for displacement measurements of case no.2

One can notice that by obtaining displacement measurements the resulting drifts do not seem to be reduced and the results are overall unaffected compared to solely obtaining acceleration measurements as presented before. Although, this effect could be conditioned on the loading and the measurement combination in this case as well as the value of the state covariance that dictates at what degree the state will be updated based on the current measurement.

3.2.5 Effects of the Covariance matrices

As proposed in the formulation of the methodology of the DKF previously, the covariance matrices Q^x and Q^p serve as the tuning knob of the system and provide a tool to furnishing the estimates based on the measurements provided each time for the system. Bearing that in mind the state process equations namely Eq. (13) and Eq. (14) are reintroduced.

$$\boldsymbol{x}_{k+1} = \boldsymbol{A}\boldsymbol{x}_k + \boldsymbol{B}\boldsymbol{p}_k + \boldsymbol{v}_k^x$$

$$\boldsymbol{d}_k = \boldsymbol{G}\boldsymbol{x}_k + \boldsymbol{J}\boldsymbol{p}_k + \boldsymbol{w}_k$$

These equations correspond to the problem being solved through the matrices **K, M** and **C** and in case where a modal analysis is needed to suppress the computational cost, Eq. (1) can be formed in terms of a modal truncated subspace:

$$\boldsymbol{\zeta}_{k+1} = \boldsymbol{A}\boldsymbol{\zeta}_k + \boldsymbol{B}\boldsymbol{p}_k + \boldsymbol{v}_k^{\zeta}$$

$$\boldsymbol{d}_k = \boldsymbol{G}\boldsymbol{\zeta}_k + \boldsymbol{J}\boldsymbol{p}_k + \boldsymbol{w}_k$$

Where v_k^x is the process noise assumed, zero-mean white with Covariance Q^x and w_k is the zero mean, white, measurement noise with covariance$R$. The two processes are mutually uncorrelated. Also, the unknown input is calibrated through the fictitious process equation :

$$\boldsymbol{p}_{k+1} = \boldsymbol{p}_k + \boldsymbol{v}_k^p$$

Where v_k^p is a zero mean white Gaussian process with it's associated covariance matrix Q^p.

By fine tuning the values of the Covariance matrices one can obtain better estimates and eliminate the drifts associated.

The effects of these values were initially introduced in case no.1 with the tuning of the noise Covariance of the measurement. Herein the effects of the selection of these values are illustrated for case no.2 and a general methodology is then proposed for a systematic scheme of selection of these values.

In that respect case no.2 is revisited and several combinations of the Covariances are implemented as presented in the following table:

For an initial value of the state Covariance matrix $Q^x = 10^{-30}$ and for two different values of the input Covariance, namely $Q^p = 10^{-5}$ and $Q^p = 10^{-1}$ responses of two indicative degrees of freedom are plotted in cross comparison as illustrated in Fig 3.13 and 3.14

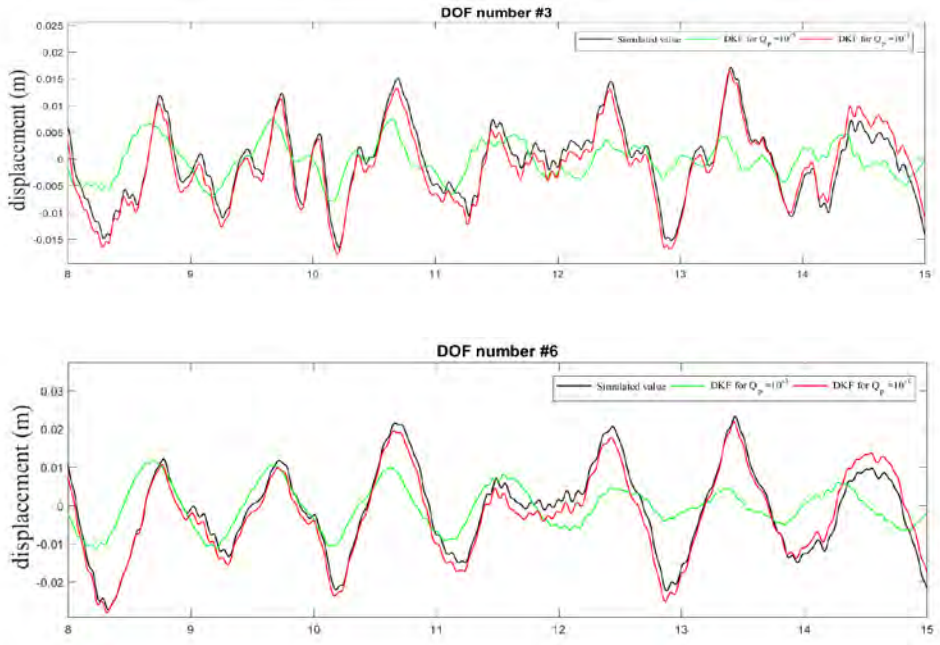

Figure 3.13: Displacement time histories for time t = 8 – 15 sec for case no.2 for the 3rd and 6th degree of freedom

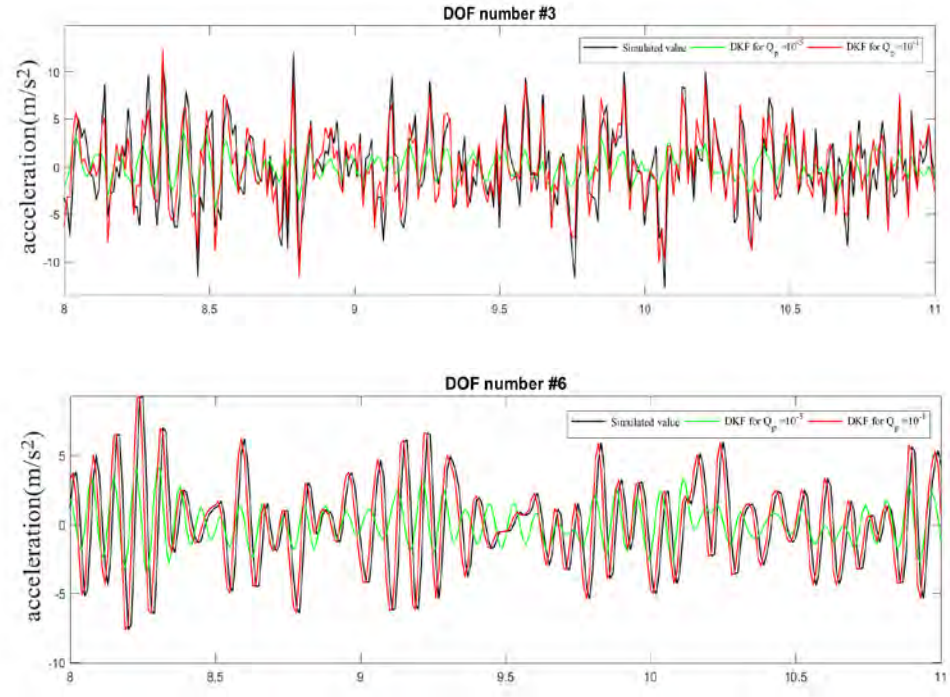

Figure 3.14 : Acceleration time histories for time t = 10 - 11 sec for case no.2 for the 3rd and 6th degree of freedom

The same process is repeated but now with an initial value of the state Covariance matrix $Q^x = 10^{-10}$ with the following results.

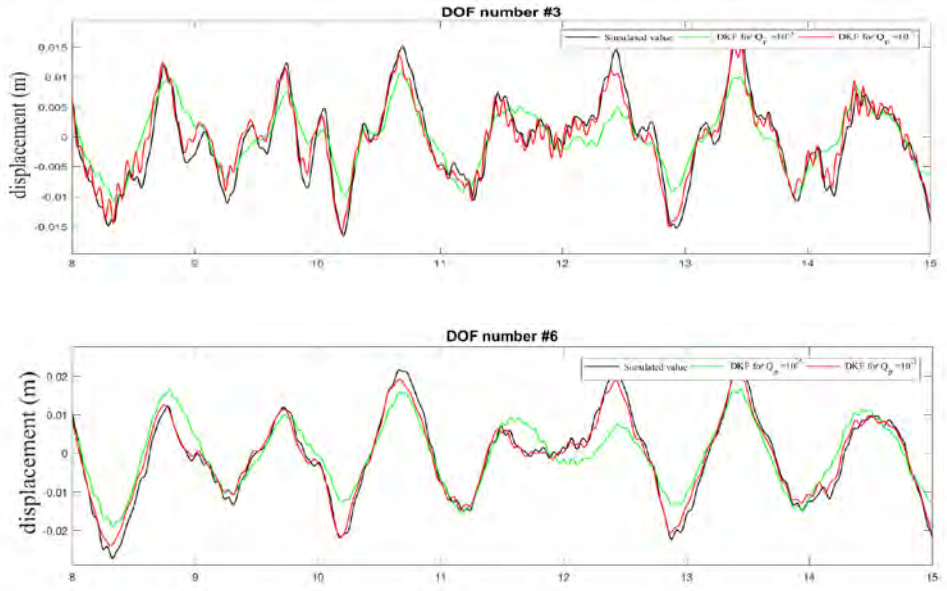

Figure3.15: Displacement time histories for time t = 8 – 15 sec for case no.2 for the 3rd and 6th degree of freedom

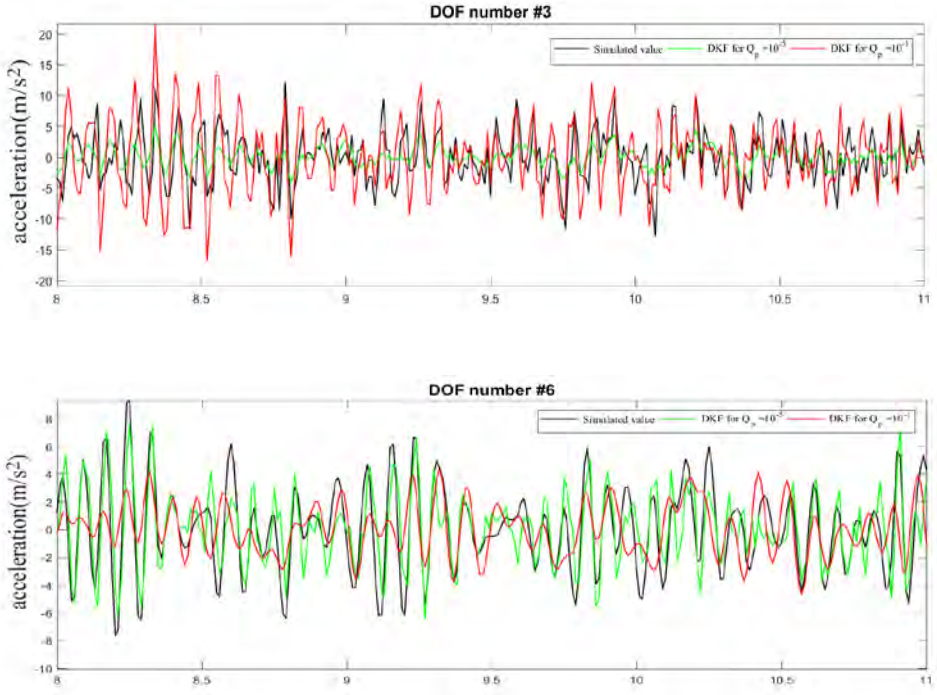

Figure 3.16: Acceleration time histories for time t = 10 - 11 sec for case no.2 for the 3rd and 6th degree of freedom

Regarding the input estimation, for the two different values of $Q^x = 10^{-30}$ and $Q^x = 10^{-10}$ the results are presented in Fig.3.17 in order to conclude the current analysis.

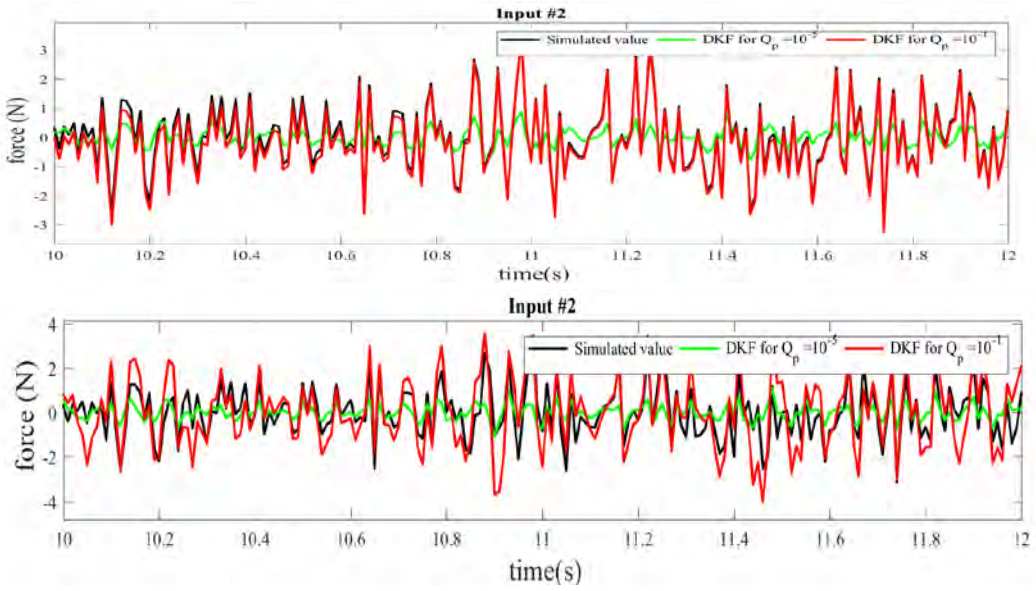

Figure 3.17: 2nd Force time histories estimates for t = 10 – 12 sec for $Q^x = 10^{-30}$ and $Q^x = 10^{-10}$ respectively

Concluding, by careful examination of the different variants of the Covariance values, one can conclude that they severely affect the estimation and thus the performance of the DKF. Moreover, one can notice that by keeping a constant value for Q^x and differentiating between certain values of Q^p one can find an optimum value that minimizes the discrepancy between the estimation and the simulated value in terms of displacements. The same applies for the estimated values of the input forces .

Also, for different values all parameters of estimation are affected. In this case by increasing the value of Q^x i.e. the confidence given to the model, one obtains slightly better estimates for the displacements but the corresponding values for the input and the accelerations are deteriorating. Therefore, it is imperative to find the optimal combination of values $Q^p and\ Q^x$ in order to obtain an overall good estimate for the sought for parameters of estimation.

In that respect, rather than arbitrarily selecting values for the Covariances a more systematic method is proposed.

3.2.6 Tuning the Covariance matrices

The main tool for minimizing the discrepancy between estimated and actual parameter is the mean squared error (***MSE***) between the observed and estimated parameter of the state of the system. Mathematically this is formulated as the following second norm which corresponds to the square novelty term in the Kalman Filter:

$$\boldsymbol{MSE} = \frac{\sum \| d_k - G\zeta_{\kappa}^{-} - J\,\widehat{p_k} \|_2^{\,2}}{N_t} \tag{17}$$

Where d_k stands for the acceleration measurements at the observed degrees of freedom at k^{th} time instance of the signal. The term $G\zeta_{\kappa}^{-} - J\,\widehat{p_k}$ stands for the output values of estimation within the Kalman Filter and N_t is the length of the signal. One can calculate the values of the ***MSE*** for a certain value of Q^x and for different values of Q^p in order to acquire an L- curve shaped diagram from which intuitively can select the proper value of Q^p as the one that minimizes the ***MSE***.

Revisiting Case no.2a the L-curve can be created for different values of the state covariance in order to investigate the optimum value of Q^p conditioned each time on the value of Q^x. The values selected in this case are the following:

$\boldsymbol{Q^x}$ = 10^{-30} , $10^{-20}$and 10^{-15} and for each L-curve Q^p spans from 10^{-20} to $10^{\,20}$.

By observing the L-curve one it is noticeable that for values of Q^p between 10^{-20} to 10^{-2} the error ordinate seems to be stable and between 10^{-2} and 10^{-8} the error norm increases rapidly until destabilizing at a higher value for decreasing Q^p beyond 10^{-8}. For an intuitive observation of the L-curve the crucial value for the force process should be the minimum one after which the error rapidly increases. In that sense, one can notice from Fig.3.18 that the crucial value that reduces the MSE lies between $Q^p = 10^{-2}$ and $Q^p = 10^{-1}$.

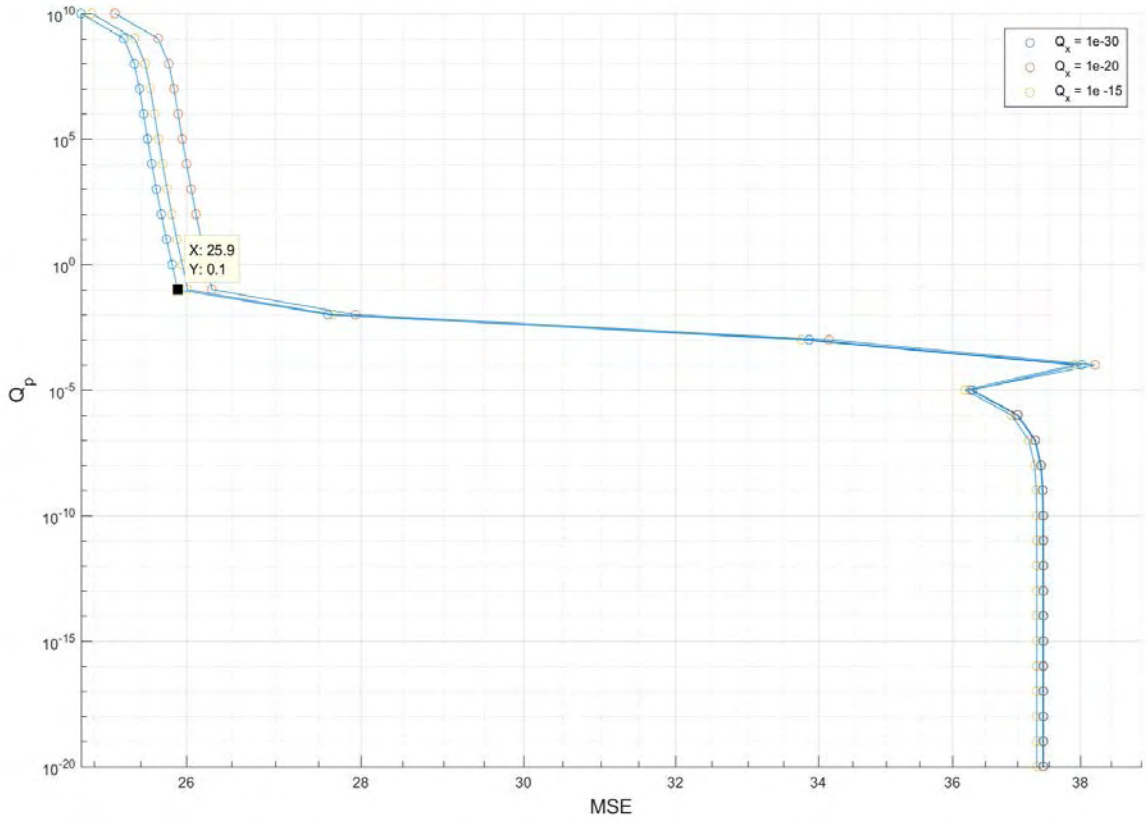

Fig. 3.18: L_curve for case no.2 for different values of the state covariance

The state process on the other hand should be predetermined and be associated with the confidence put in the mathematical representation of the physical system at hand. Therefore, manipulating these values may produce low errors in the L-curve but consist a misconception and produce false results in regards of the estimates.

Last but not least, the ordinate of the error seems to attain a high value even for an optimum covariance selection due to the fact that measurements are not obtained at all points where the forces are applied.

3.2.7 Case no.3 - Modal analysis

In this section of the analysis the efficiency of the DKF is evaluated in the case of a modal analysis approach. As presented in Eq. (6) the equations of motions can be reformulated in order to introduce a coordinate transformation using the eigenvalues, the eigenvectors and the damping ratio of the system. This transformation enables to reduce the order of the system i.e. truncated model and consider the response as a superposition of some undamped modes.

For that purpose, a new system is introduced similar to the one in the previous analysis which now is consisted of 20 degrees of freedom.
The system is subject to 3 non – collocated forces where measurements are obtained from.

Simulation parameters	
Number of loads = 2	DOF
Load #1	5^{th}
Load #2	9^{th}
Load #2	12^{th}

Table 3.5: Simulation parameters for modal analysis case

DKF parameters	
Number of observations = 2	DOF
Observation of accelerations	5^{th} 9^{th} 12^{th}
Observation of displacements	5^{th} 9^{th} 12^{th}

Table 3.6: DKF parameters for modal analysis case

The natural frequencies are presented as following:

Vibration mode index	Natural frequency (Hz)
1	0,52541
2	1,57316
3	2,61168
4	3,63487
5	4,63673
6	5,61137
7	6,55309
8	7,45640
9	8,31586
10	9,12656
11	9,88371
12	10,5829
13	11,2199
14	11,7911
15	12,2931
16	12,7230
17	13,0782
18	13,3567
19	13,5567
20	13,6772

Table 3.7:Natural frequencies of 20 DOF sytem

The initial values of the Covariance of the diagonal components of the state Covariance matrix are set at $Q^x = 10^{-20}$ whereas the corresponding values of the Input Covariance are set at $Q^p = 10^{-1}$.

In order to determine which modes contribute to the response of the system, the power/frequency spectrum is plotted for the measurement of the 9th degree of freedom.

By a closer examination of the power spectral density in Fig 3.19 and 3.20 one notices that all of the eigenfrequencies of the system are excited. This is part to the fact that the inputs loads for the purpose of this analysis, are simulated as White noise Gaussian processes and therefore attain constant power spectral density over all the frequencies of the system. Hence, in this case all the modes of the system should be superpositioned in order to obtain a reasonable estimate for the response.

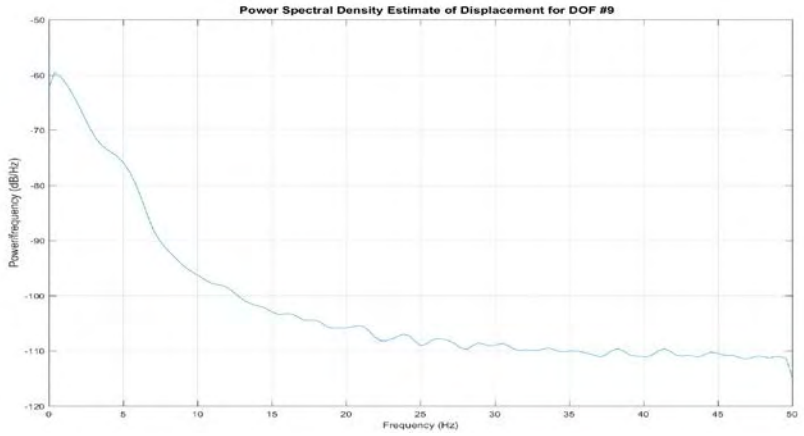

Fig 3.19: Power Spectral Density estimate of the Displacement of 9th degree of freedom

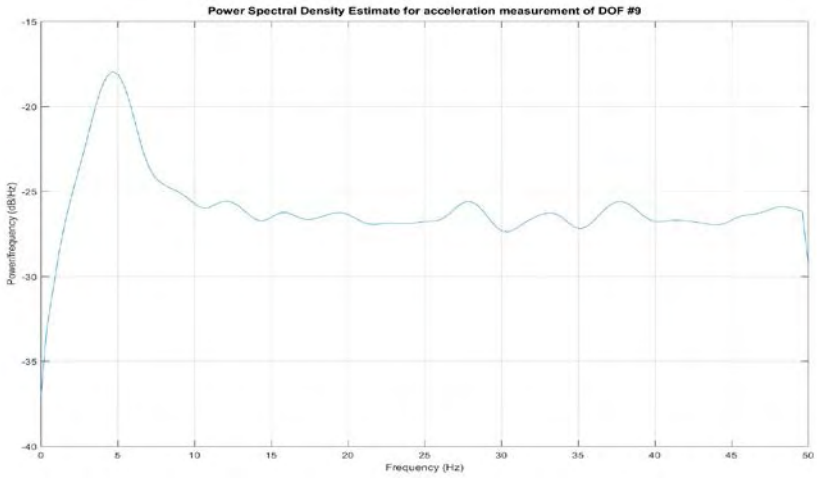

Fig 3.20 . Power Spectral Density estimate of the acceleration of 9th degree of freedom

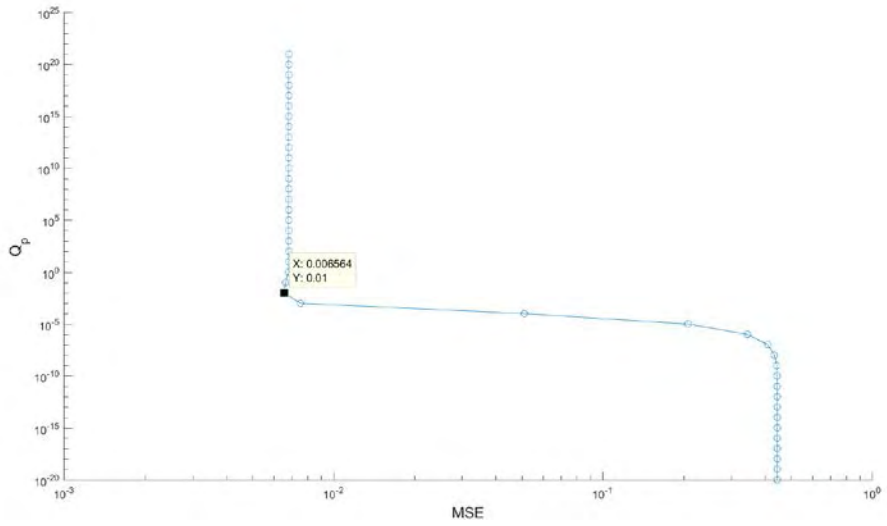

Fig. 3.21: L-curve for modal analysis case

Also, the L – curve is plotted in order to ensure that the selection of the covariance of the force process is appropriately selected. The optimal value seems to lie between 10^{-3} and 10^{-2}.

The results of the estimation are presented in Fig 3.23 and 3.24 as follows with estimated responses on both measured and non-measured degrees of freedom.

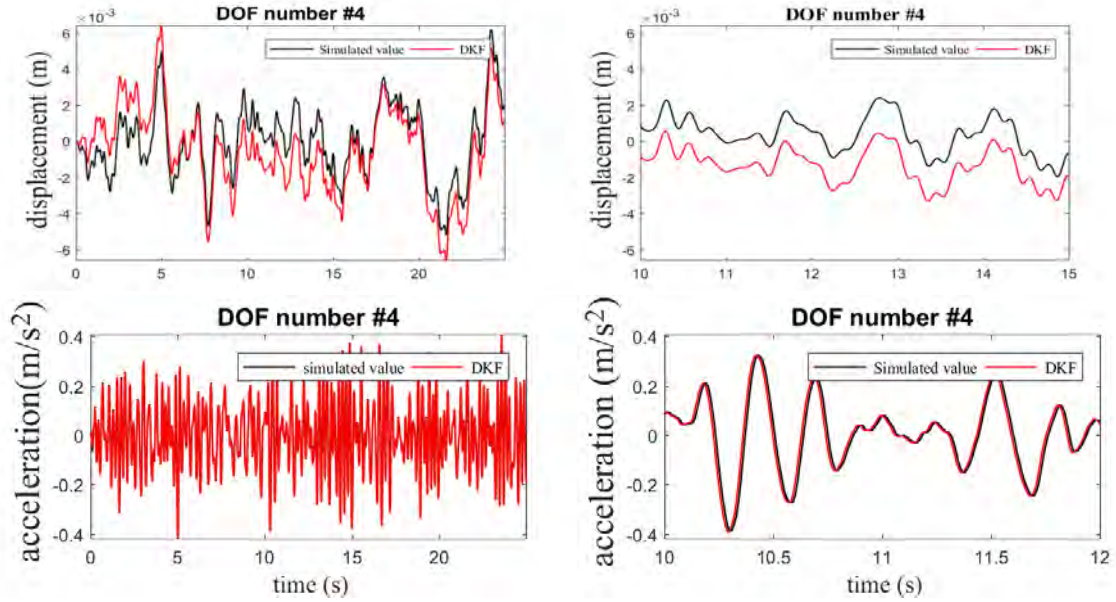

Figure 3.22: Response time histories for the unobserved 4th degree of freedom for modal analysis

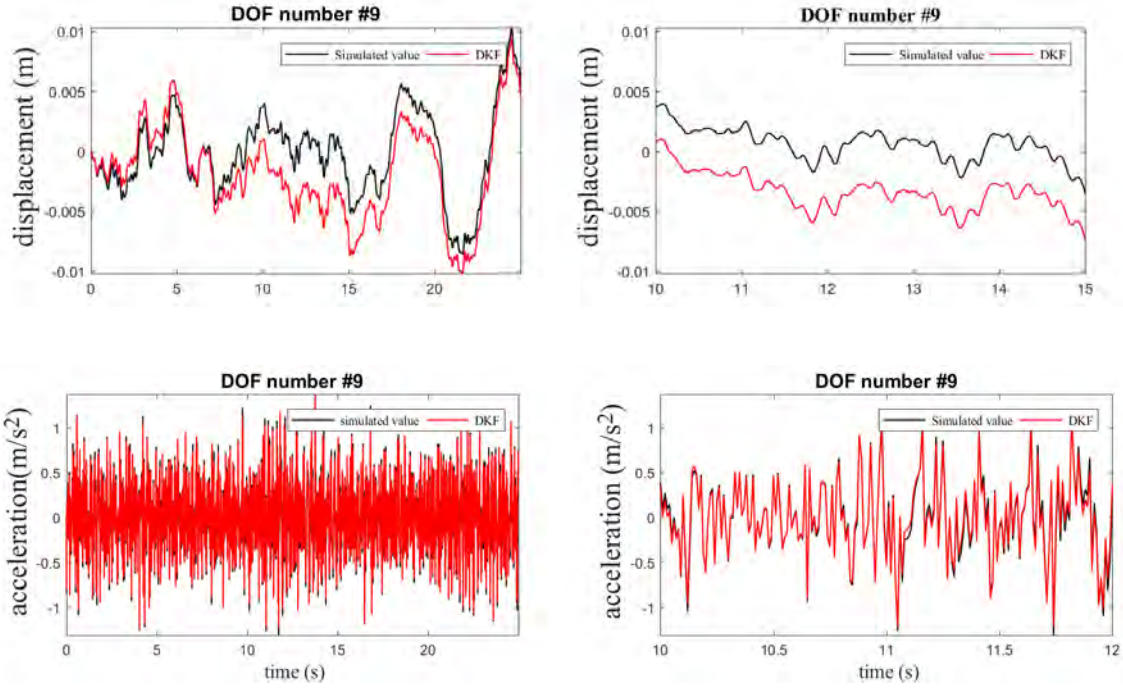

Figure 3.23: Response time histories for the observed 9th degree of freedom for modal analysis

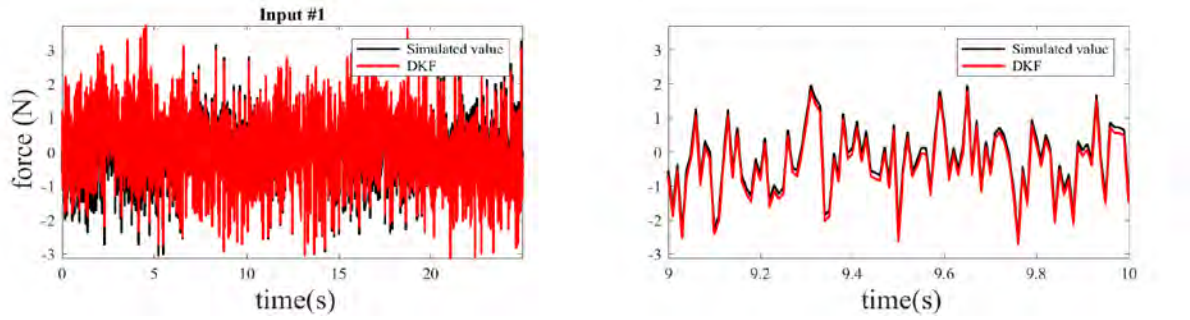

Figure 3.24: Force time history estimate for 1st Input force for modal analysis

Again, sufficient estimating accuracy is achieved for all parameters of estimation except for the displacements where significant drifts appear.

It becomes evident that when multiple collocated or non-collocated inputs, formed as Gaussian white noise, are applied at certain degrees of freedom, the so far proposed methodology of estimation provides estimates with drifts in terms of displacement.

However, the trajectories of the displacements are mutually dislocated in all degrees of freedom and their paths are followed in a sufficient way.

It is also worth noting that the modal analysis also provides an equivalent method to the one that implements the matrices **K, M** and **C** while suppressing the associated computational cost by reducing the order of the system.

In order to underline this attribute an alternative case is introduced in which the applied inputs are acting on the same measured points but are now rectangular impulses.

The power/frequency spectrum is plotted for the measurement of the 9th degree of freedom.

Close examination concludes that the first 10 eigenfrequencies are excited and that mainly the 10 associated eigenmodes of the system take part in the response of the system and they are taken into account in the DKF algorithm. As shown in Fig: 3.27 by only taking into account 10 modes of the system, accurate estimates can be achieved although with the associated drifts at the displacements encountered so far.

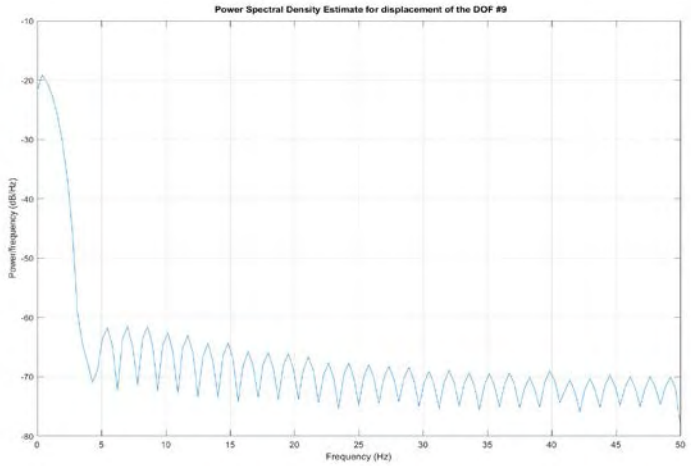

Fig 3.25 . Power Spectral Density estimate of the Displacement of 9‴ degree of freedom for rectangular excitation

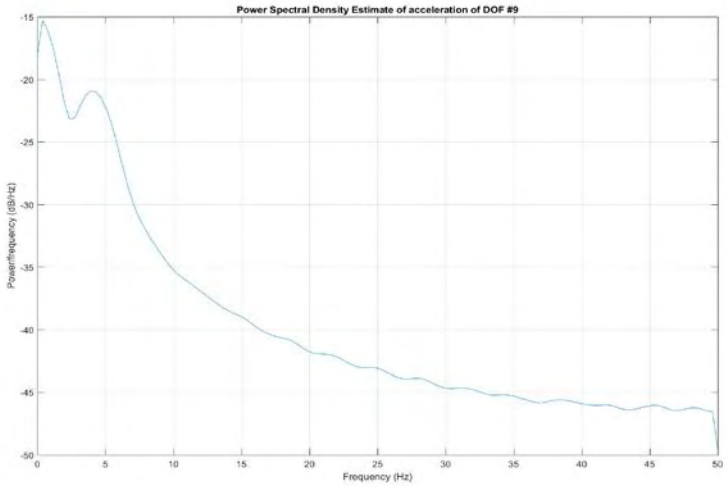

Fig 3.26 . Power Spectral Density estimate of the acceleration of 9th degree of freedom for rectangular excitation

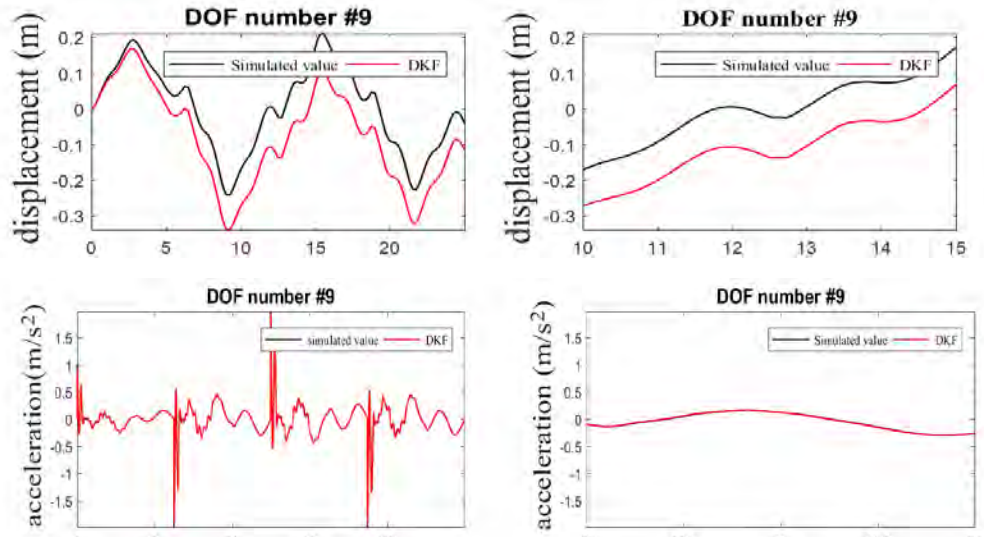

Fig 3.27 : Response time histories for the observed 9th degree of freedom in case of rectangular impulse excitation

Chapter 4

Fatigue damage accumulation

4.1 Introduction

Metallic structures tend to suffer from fatigue damage accumulation due to loading and therefore it's prediction is an important safety related parameter in structural health monitoring. Considering various loading events, stress response time histories can be obtained in various hotspots of the structure via a sensor network attached to these locations. Subsequently, cycle counting methods such as Rainflow counting method can be used in order to reduce the varying amplitude stresses into a set of simple stress reversals. This in turn, allows the calculation of the lifetime prognosis of the structure through the use of the linear Palmgren-Miner rule and data obtained from the S-N curves obtained from laboratory experiments of simple specimens subjected to constant amplitude loads.

In many engineering applications, though it is not possible to obtain measurements at all hotspot locations due to practical and economical reasons. Such cases are heated components or internal points of the structure. In that respect only a limited number of acceleration measurements are available and therefore a Kalman filter implementation is proposed in order infer damage due to fatigue to unobserved locations of the structure. This can be achieved by coupling the measurements with the dynamic model of the structure in a stochastic process framework.

In this section, an implementation of the Kalman filter is used to make such estimates and evaluate it's estimating efficiency in case of multiple loads and for cases in which the measurements are obtained at locations where the loads are not applied.

4.2 Mathematical formulation of fatigue damage prognosis

As stated previously, the Palmgren-Miner method can be introduced to calculate the remaining timelife of the structure, which follows that:

$$\boldsymbol{D_j} = \sum_{i=1}^{k} \frac{n_i}{N_i}$$

where $\boldsymbol{D_j}$ is the damage accumulation at point $j$of the structure and k stands for the number of loading events. Also, n_i is the is the number of cycles under stress level s_i and N_i the number of cycles required for failure under the same stress level.

Number of cycles n_i can be calculated through stress cycle counting methods such as Rainflow cycle counting which is used in this case whereas N_i can be obtained from laboratory experiments and the formulation of $S-N$ curves. The stress cycle ranges are modified through the Goodman relationship:

$$\Delta s_{Rt} = \Delta s_R(1 - \frac{\sigma_m}{\sigma_{ts}})$$

where Δs_{Rt} is the modified stress cycle range, σ_m is the mean stress, Δs_R is the fatigue limit for completely reversed loading, and σ_{ts} is the ultimate tensile strength of the material. Eq. * is substituted into Eq. and the rule of fatigue Damage becomes:

$$\boldsymbol{D_j} = \sum_{i=1}^{k_1} \frac{n_i}{N_f} \frac{\Delta s^m}{\Delta s_D^m} + \sum_{i=1}^{k_2} \frac{n_j}{N_f} \frac{\Delta s_j^{m+2}}{\Delta s_D^{m+2}}$$

where k_1 and k_2 correspond to the different stress range blocks above and below the constant amplitude fatigue limit Δs_D. The cut off limit is set to be Δs_L and the first term applies for$\Delta s_D \leq \Delta s_j$ whereas the second for $\Delta s_L \leq \Delta s_j \leq \Delta s_D$.

4.3 Fatigue damage accumulation using Kalman Filtering

The above proposed methodology is implemented for the following properties of the model:

Model Properties
$\boldsymbol{Ndof = 10}$
$\boldsymbol{M = 0.35\,kg}$
$\boldsymbol{K = 600\,N/m}$
$\boldsymbol{\zeta = 5\%}$

Table 4.1: Model properties

The fatigue analysis has been implemented under the Material reference Eurocode for steel structures [13] for material with detail category 36 with the following specifications:

$m^* = 3$ *slope of fatigue strength curve*	$\Delta s_L = 14.5$ *Mpa*
$L = 3$ *meters*	$\Delta s_D = 26.5$ *Mpa*
$E = 210 * 10^3$ *Mpa*	$\sigma_{ts} = 100$ *MPa*

Table 4.2: Fatigue properties

$^*N_f = 10^6$ *infinite life cycle*

	DOF			
	# Inputs	Input(s)		Measurement	
Case no.4	1	9th		9th	
Case no.5	2	4th	8th	4th	8th
Case no.6	3	5th	9th	6th	10th

Table 4.3: Different cases of loading and measurement

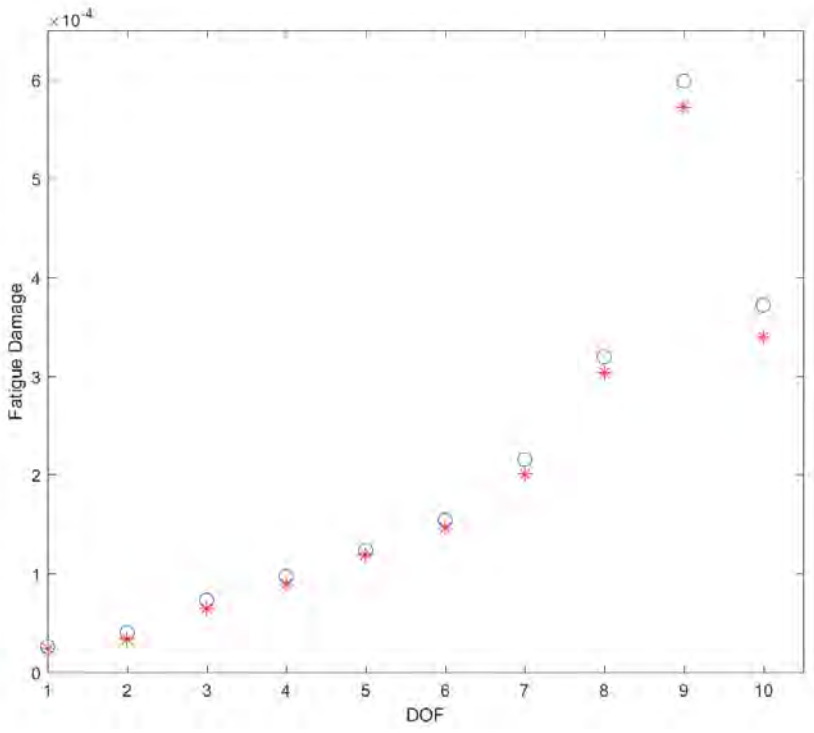

Fig 4.1 . Fatigue damage accumulation for case no.5

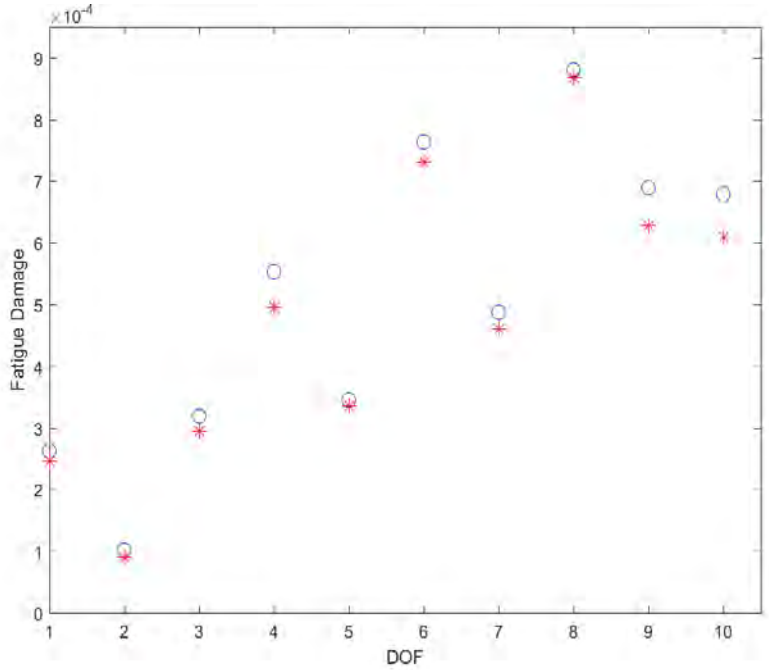

Fig 4.2 . Fatigue damage accumulation for case no.5

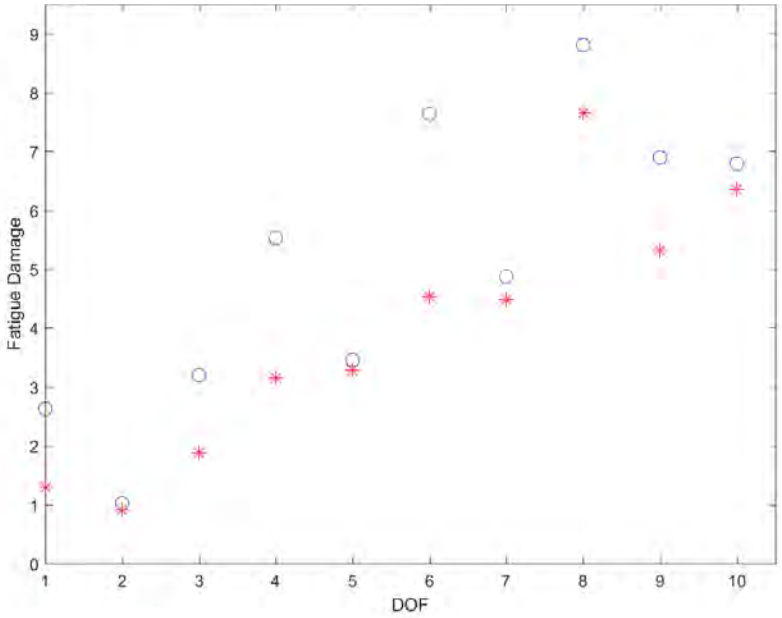

Fig 4.3. Fatigue damage accumulation for case no.6

In respect to the estimating efficiency of the DKF as far as the fatigue damage is concerned, the DKF algorithm produces the expected results in an equivalent manner as in the displacements. Since the strains are proportional to the consecutive relative displacements of the corresponding degrees of freedom, the estimating efficiency will be conditioned on

the estimation of displacements. Therefore in cases that the observed points are different than the ones where the forces are applied inaccurate estimates will be obtained. On the other hand, drifts that arise as number of inputs increases do not deteriorate the estimates.

Lastly, as expected the degrees of freedom that suffer more in the current thesis are the ones that the forces are applied to since this is a simple spring mass linear mode. However, in cases of more complex structures, hotspots could be ones not directly subject to forces.

Chapter 5

Input and state prediction using model Substructuring

5.1 Mathematical Formulation

The structural dynamics problem, which is herein studied, is the one of the substructured system.

An initial n degree of freedom system is considered and is excited by a force at its base as indicated in the following figure.

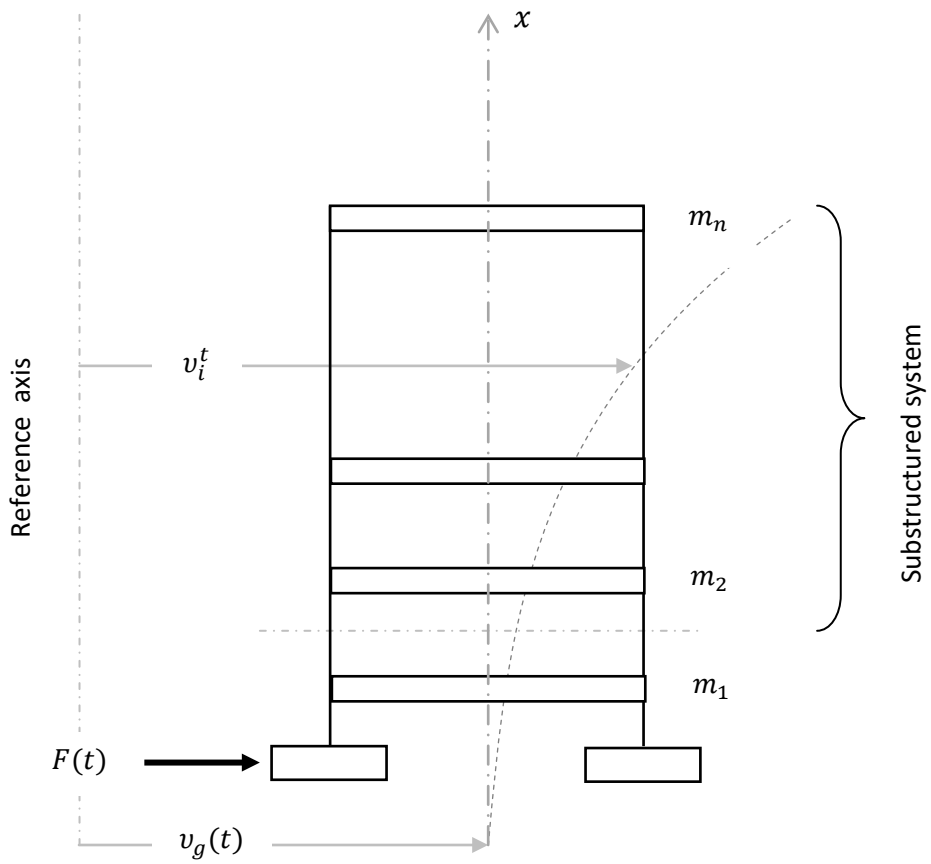

Fig. 5.1: Schematic representations of Substructure

A subsequent subsystem is then obtained, which contains the $n-1$ degrees of freedom of the initial system.

The new system now is not subjected to external forces and the excitation comes from the response of the subtracted degree of freedom, which now acts as an equivalent ground support excitation. This can be derived by expressing the total displacement as the sum of the relative motion plus the displacements resulting from the support motions.

Let $\boldsymbol{u}^t(t)\epsilon\, R^n$ be a vector containing the total displacements v_i^t of each degree of freedom. As shown in the figure the aforementioned relationship can be written as following.

$$\boldsymbol{u}^t(t) = \boldsymbol{u}(t) + \{\mathbf{1}\}\,\boldsymbol{v_g}(t) \tag{18}$$

in which in which **{1}** represents a column of ones. This vector expresses the fact that a unit static translation of the base of this structure produces directly a unit displacement of all degrees of freedom. This hypothesis is applicable only to a certain types of support displacement as well as the type of structural configurations but has nonetheless significant numerous applications.

The governing equation of the structural dynamics problem for the substructured system is typically formulated, as studied previously, using the following continuous time second order differential equation:

$$\boldsymbol{M\ddot{u}^t} + \mathbf{C}\dot{\boldsymbol{u}} + \boldsymbol{Ku} = \mathbf{0} \tag{19}$$

Substituting eq. (17) to eq. (18) one gets:

$$\boldsymbol{M\ddot{u}^t}\,(t) + \mathbf{C}\,\dot{\boldsymbol{u}}^t(t) + \mathbf{K}\boldsymbol{u}^t(t) = \boldsymbol{K}\,\{\mathbf{1}\}\,\boldsymbol{v_g}(t) + \mathbf{C}\{\mathbf{1}\}\,\dot{\boldsymbol{v}}_g(t) \tag{20}$$

Eq. (19) can now be transformed into :

$$\boldsymbol{M\ddot{u}^t}\,(t) + \mathbf{C}\,\dot{\boldsymbol{u}}^t(t) + \mathbf{K}\boldsymbol{u}^t(t) = \boldsymbol{S_p p}(t) \tag{21}$$

where $\boldsymbol{S_p}\,\epsilon\, R^{2n\,x\,2}$ is the influence matrix indicating the load distribution at certain degrees of freedom of the system and $\boldsymbol{p}(t)$ are the load time histories.

This is the typical form encountered so far, but now :

$$\boldsymbol{S_p} = [\boldsymbol{K}\,\{\mathbf{1}\}\,\mathbf{C}\{\mathbf{1}\}] \quad \textit{and}$$

$$\boldsymbol{p}(t) = \begin{bmatrix} \boldsymbol{v_g}(t) \\ \dot{\boldsymbol{v}}_g(t) \end{bmatrix}$$

Introducing the state vector $\boldsymbol{x}(t) = \begin{bmatrix} \boldsymbol{u^t}(t) \\ \dot{\boldsymbol{u}}^t\,(t) \end{bmatrix}$ where $\boldsymbol{x}(t)\epsilon\, R^{2nx1}$ equation (4) can be transformed into a first order continuous-time state equation as encountered previously:

$$\dot{\boldsymbol{x}}(\boldsymbol{t}) = \boldsymbol{A_c x}(t) + \boldsymbol{B_c p}(t)$$

where $\boldsymbol{A_c} \in R^{2nx2n}$ and $\boldsymbol{B_c}$ $\in R^{2nx2}$ are the following matrices :

$$\boldsymbol{A_c} = \begin{bmatrix} \boldsymbol{0} & \boldsymbol{I} \\ \boldsymbol{-M^{-1}K} & \boldsymbol{-M^{-1}C} \end{bmatrix}$$

$$\boldsymbol{B_c} = \begin{bmatrix} \boldsymbol{0} \\ \boldsymbol{M^{-1}S_p} \end{bmatrix}$$

Regarding the measurement equation a general case of a vector $\boldsymbol{d}(t) \in R^{n_o x1}$ containing displacement, velocity and acceleration measurements is considered.

$$\boldsymbol{d}(t) = \begin{bmatrix} \boldsymbol{S_d} & \boldsymbol{0} & \boldsymbol{0} \\ \boldsymbol{0} & \boldsymbol{S_v} & \boldsymbol{0} \\ \boldsymbol{0} & \boldsymbol{0} & \boldsymbol{S_a} \end{bmatrix} \begin{bmatrix} \boldsymbol{u^t}(t) \\ \boldsymbol{\dot{u}^t}\,(t) \\ \boldsymbol{\ddot{u}^t}(t) \end{bmatrix}$$

Where $\boldsymbol{S_d}, \boldsymbol{S_v}, \boldsymbol{S_a}$ $\in R^{n_d x\, n}$ are the selection matrices of appropriate dimension for the displacements, velocities and accelerations respectively. The term n_d stands for the number of observations of displacements, velocities and accelerations for each of component. These matrices identify which degree of freedom measurements are taken from and in this thesis mainly accelerations and displacement measurements are used.

The equivalent state space form of the measurement vector can be given by

$$\boldsymbol{d}(t) = \boldsymbol{G_c}\, \boldsymbol{x}(t) + \boldsymbol{J_c p}(t)$$

where the matrices $\boldsymbol{G_c} \in R^{n_d x\, 2n} and\, \boldsymbol{J_c} \in R^{n_d x\, 2}$ are

$$G_c = \begin{bmatrix} \boldsymbol{S_d} & \boldsymbol{0} \\ \boldsymbol{0} & \boldsymbol{S_v} \\ \boldsymbol{-S_a M^{-1} K} & \boldsymbol{-S_a M^{-1} C} \end{bmatrix} \quad \text{and}$$

$$\boldsymbol{J_c} = \begin{bmatrix} \boldsymbol{0} \\ \boldsymbol{0} \\ \boldsymbol{S_a M^{-1} S_p} \end{bmatrix}$$

Under the assumption that the sampling rate is $\frac{1}{dt}$, the continuous time equations (5) and (6) can be discritised in time in the following form:

$$\boldsymbol{x_{k+1}} = \boldsymbol{A x_k} + \boldsymbol{B p_k}$$

$$\boldsymbol{d_k} = \boldsymbol{G x_k} + \boldsymbol{J p_k}$$

Where $A = e^{\boldsymbol{A_c} dt}$, $\boldsymbol{B} = [\boldsymbol{A} - \boldsymbol{I}]\boldsymbol{A^{-1}_C}\, \boldsymbol{B_c}$, $\boldsymbol{G} = \boldsymbol{G_c}$, $\boldsymbol{J} = \boldsymbol{J_c}$

and $\boldsymbol{x_k} = \boldsymbol{x}(kdt)$, $\boldsymbol{p_k} = \boldsymbol{p}(kdt)$, $\boldsymbol{d_k}$ = $\boldsymbol{d}(kdt)$.

The algorithm of the dual Kalman filter is implemented as studied in chapter.

5.2 Dual Kalman Filter approach for joint input and state estimation of substructured system

The goal now focuses on the problem of estimating the input and state of the system in order to predict the strain time histories by considering the relative response of the first as an input to the second one. The problem at hand classifies as a similar case to the ones studied in this analysis, where now the first term i.e. displacement is applied in the first degree of freedom whereas the velocity term of the first degree of freedom is applied in all degrees of freedom of the sub-structure.

At first, a force is simulated to apply on the system before the substracturing and two noisy acceleration measurements are considered in the 2nd and 3rd degree of freedom of the original system i.e. 1st and 2nd of the substructured system. Furthermore, the responses of the 1st degree of freedom are obtained to be compared with the input at the end of the analysis. The substructured model is also composed of 10 degrees of freedom and is modeled as mass-spring chain like system with the same properties introduced in the first Chapter.

The state covariance is set to be $Q^x = 10^{-20}$ where as the noise measurement Covariance is set as follows $\boldsymbol{R} = \boldsymbol{s^2} * \boldsymbol{I}$, where s is a vector containing the standard deviation of each measurement signal.

The tuning of the force process Covariance is of particular importance at this case. This is due to the fact that the two inputs forces, formulated into a stochastic process framework, are likely to have different variances and thus a more investigative L-curve investigative scheme should be implemented.

In the previous analysis it was considered that $\boldsymbol{Q^p} = Q * \boldsymbol{I}$ with $\boldsymbol{I}$ being the diagonal matrix containing ones with the appropriate dimensions.

Herein, it is considered that $\boldsymbol{Q^p} = \begin{bmatrix} Q_1^p & 0 \\ 0 & Q_2^p \end{bmatrix}$ where Q_1^p and Q_2^p correspond to the Covariances of each individual force process respectively.

In that respect, two sets of L-curves are in order to find the combination of the diagonal components of the Covariance matrix that minimizes the MSE. The two sets are each

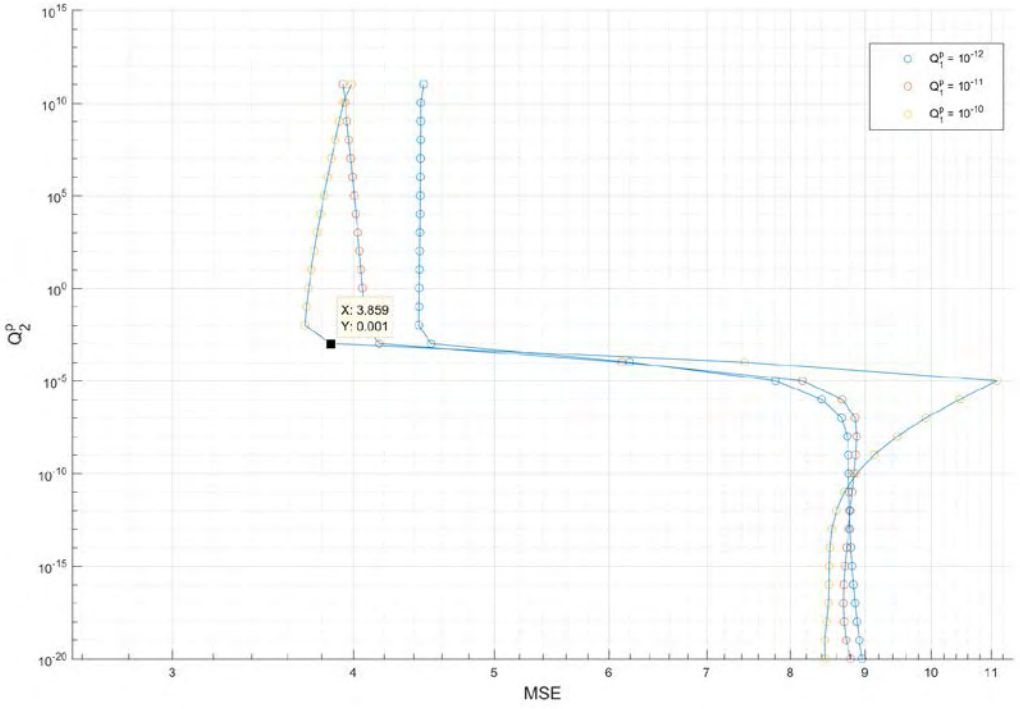

Fig5.2 . L-Curve plots of substructure model for different values of Q_1^p in respect to Q_2^p

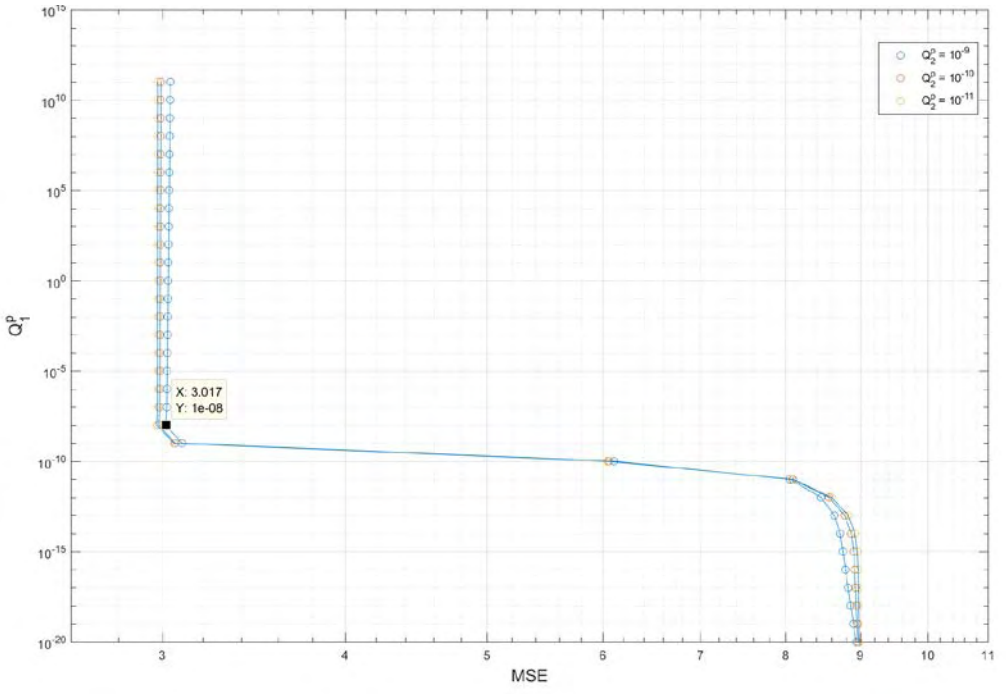

Fig 5.3 : L-Curve plots of substructure model for different values of Q_2^p in respect to Q_1^p

comprised of 42 L- curves with Covariances spanning $\boldsymbol{Q^p} = 10^{-20}\ to = 10^{20}$.

Since the values are spanning in a wide spectrum of values only some L-curves maintain the characteristic *L* shape and for the sake of clarity only the ones that produce reasonable results are plotted. Close examination of Fig. and Fig. leads to the conclusion that the most reasonable selection can be obtained from the second figure. Not only is the error minimized at a greater extent, but the L-curves in the second case seem to follow the characteristic shape in a more strict rule. Specifically, $MSE_1 \approx$ 3.9 where as $MSE_2 \approx$ 3.02. As far as the choice between the three values of Q_2^p is concerned one wishes to obtain the maximum value after which the error is minimized and not drastically affected.

Taking into consideration the aforementioned reasoning the most suitable subset of values for the force process Covariance would be :

$Q_1^p = 10^{-8}$ and $Q_2^p = 10^{-9}$ with a corresponding MSE of 3.017.

The input estimates are presented as follows:

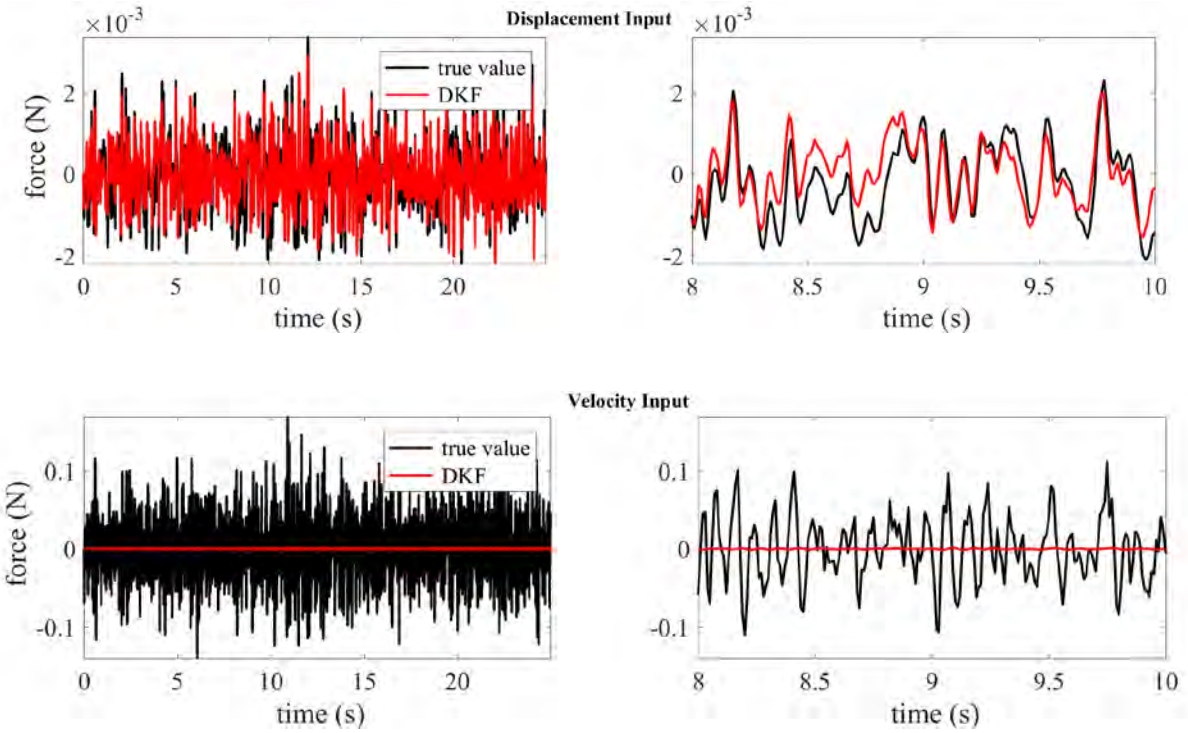

Fig 5.4 : Force estimates for the substructured system

As seems evident the proposed scheme can only achieve an accurate estimate only for the displacement while no result is produced for the velocity input.

Nonetheless, reasonable estimates are obtained in respect of all accelerations as indicatively presented in Fig 5.5 for the first degree of freedom:

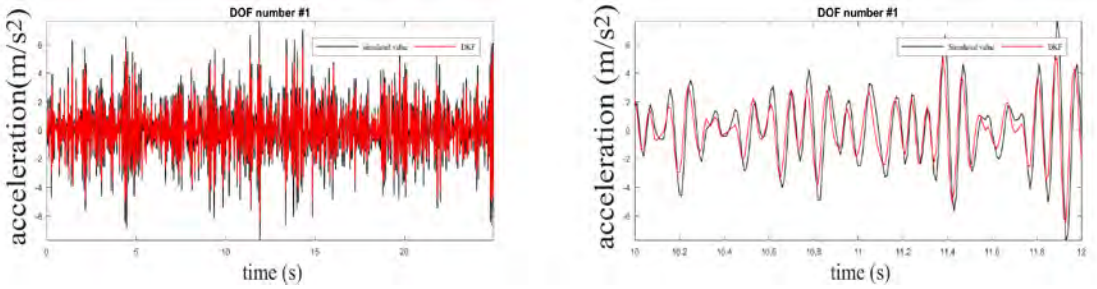

Fig 5.5 : Acceleration time history estimate for the 1st degree of freedom

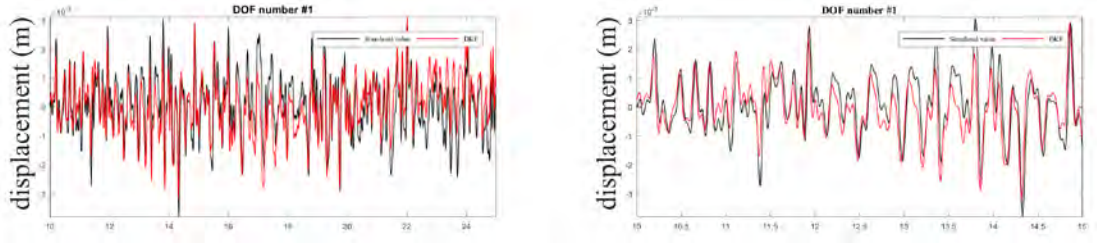

Fig 5.6 : Displacement time history estimate for the 1st degree of freedom

Adopting the same methodology developed in Chapter 4, the stress and strain time history estimates can be produced with high accuracy in this case.

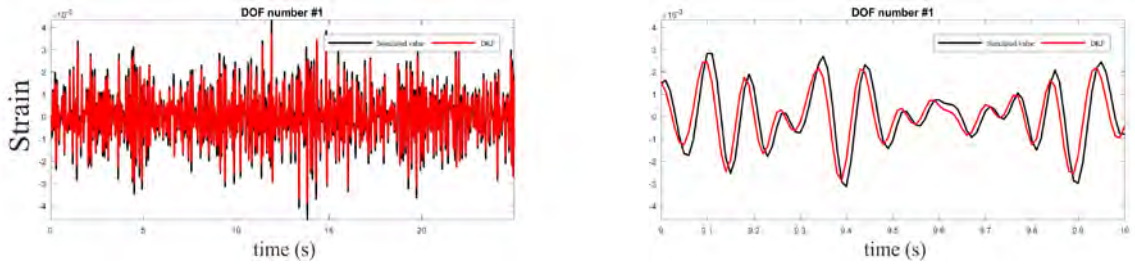

Fig 5.7: Strain time history estimate for the 1st degree of freedom

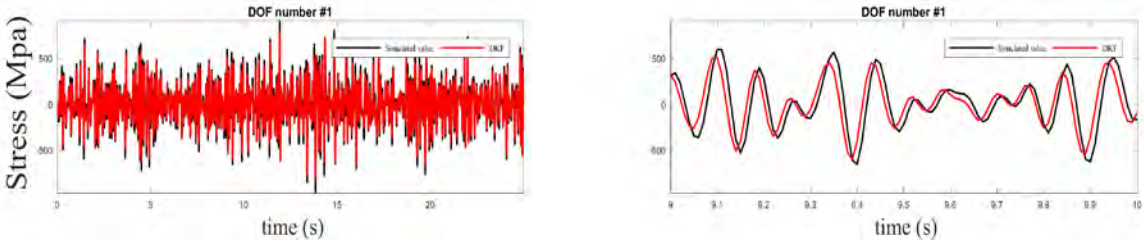

Fig 5.8: Stress time history estimate for the 1st degree of freedom

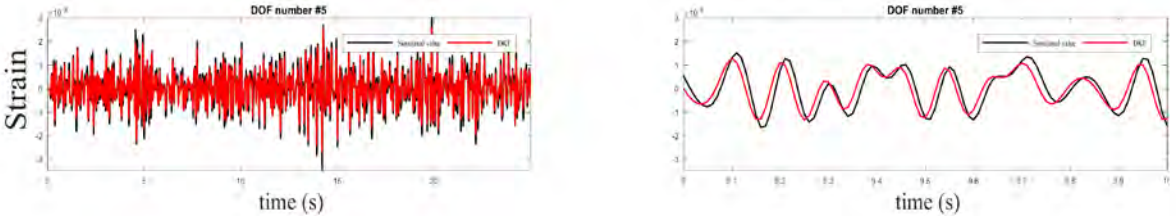

Fig 5.9 : Strain time history estimate for the 5th degree of freedom

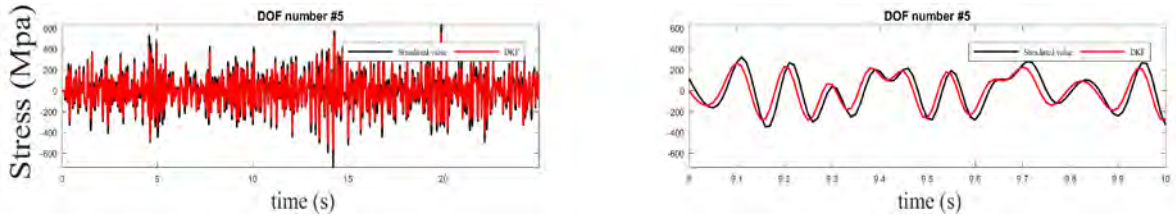

Fig 5.10: Stress time history estimate for the 5th degree of freedom

Concluding, the fatigue damage accumulation all over the structure can be estimated with a relative margin of error especially on the 1st degree of freedom where both terms of velocity and displacement are applied.

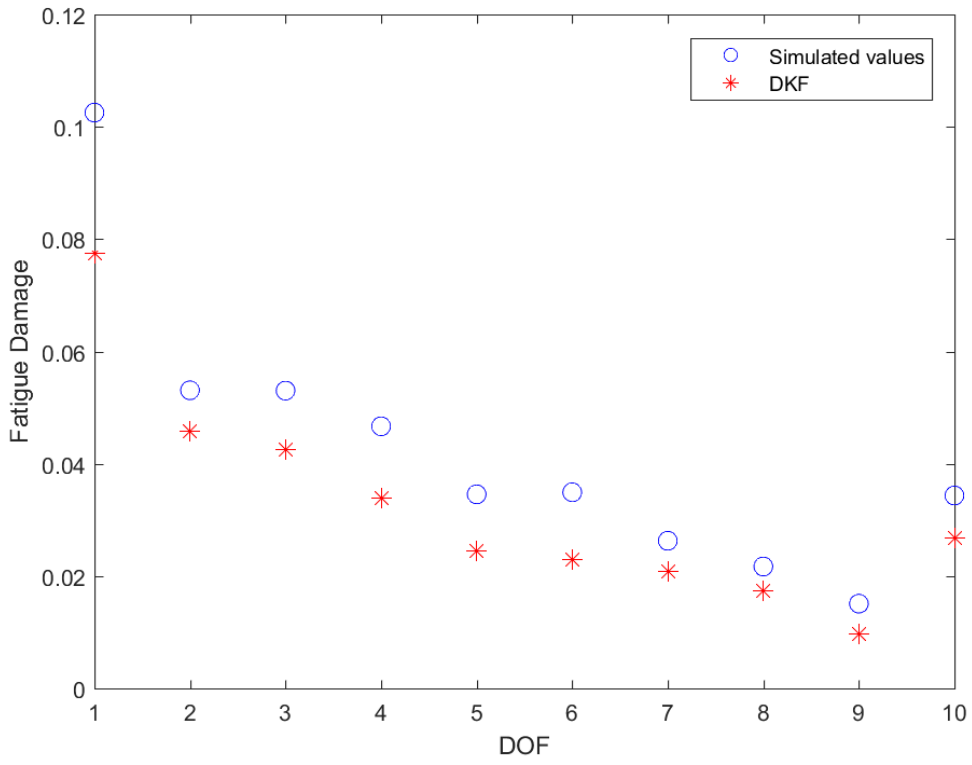

Fig 5.11 : Fatigue damage accumulation estimate on substructured system

In order to further improve the estimates several other combinations of measurements could be acquired in the scope of maximizing the information obtained regarding the states.

One last way to alleviate the lack of estimation would be to consider the input of displacement known as estimated and then attempt to estimate the velocity term through the used so far Kalman filtering methodology.

Chapter 6

Conclusion

In this work a dual implementation of a Kalman filtering scheme was used in order to jointly estimate the state and the input of a spring mass chain like model. It was shown that the degree of estimating accuracy is heavily conditioned on the knowledge of the location of the applied inputs and subsequently the location of the measurements. The lack of knowledge seems to deteriorate the estimates on the states while on the other hand reasonable results can be produced in terms of input when measured locations identify with load locations. The number of inputs in non collocated cases should not be greater than the number of applied forces. Furthermore, the effects of the values of the diagonal components of the Covariances on the parameter estimation were studied and systematic methods of tuning these values were implemented. It was shown that the state Covariance should be correctly identified in a model identification framework before attempting to estimate while the measurement and force process Covariances served as the tuning knobs of the estimating scheme. The efficiency of a modal analysis of a truncated system was also proven and a fatigue analysis was put forward in order to locate the hotspot locations of the system under uncertain loading. Lastly, the developed methodology was applied in a substructured system of the original $n\ dof$ structure in where the responses of the first degree of freedom were introduced as inputs on the substructured system. Responses, stress time histories and subsequently fatigue analysis estimates were produced with sufficient level o accuracy.

The current strategy could be improved by proposing a more systematic scheme of obtaining the maximum information for the input and the states through the measurements. In other words, an optimal measurement combination could improve the estimating efficiency coupled with new tuning techniques. Lastly, a modified DKF procedure could be developed in order to consider only some of the inputs known and attempt to estimate the remaining unknown ones.

Literature

[1] Saeed Eftekhar Azam, E. Chatzi, C. Papadimitriou, A dual Kalman filter approach for state estimation via output-only acceleration measurements, Mechanical Systems and Signal Processing (2015)1-21.

[2] Saeed Eftekhar Azam, Eleni Chatzi, Costas Papadimitriou, and Andrew Smyth.Experimental validation of the Kalman-type filters for online and real-time state and input estimation, *Journal of Vibration and Control* Vol 23, Issue 15, pp. 2494 - 2519

[3] R.E. Kalman, A new approach to linear filtering and prediction problems,J.Basic Eng.82(1960)35–45

[4] N.J. Gordon,D.J.Salmond,A.F.M.Smith, Novel approach to nonlinear/non-Gaussian Bayesian state estimation,IEEProc.-F:RadarSignalProcess.140 (1993)107–113.

[5] S. Gillijns, B. De Moor, Unbiased minimum-variance input and state estimation for linear discrete-time systems with direct feedthrough, Automatica 43 (2007) 934-937.

[6] S.Bittanti, S. M. Savaresi, On the parameterization and design of an extended Kalman filter frequency tracker, IEEE Trans. Autom. Control 45 (2000) 1718-1724.

[7] M.R. Rajamani, J. B. Rawlings, Estimation of the disturbance structure from data using semidefinite programming and optimal weighting, Automatica 45 (2009) 142-148.

[8] M.A. Miner, Cumulative damage in fatigue, Applied mechanics Transactions (ASME) 12 (3): A159-A164 (1945).

[9] A. Palmgren, Die Lebensdauer von Kugallagern, VDI-Zeitschrift 68(14):339-341 (1924).

[10] C. Papadimitriou, C. P. Fritzen, P. Kraemer, E. Ntotsios, Fatigue predictions in entire body of metallic number of vibration sensors using Kalman filtering, Struct. Control Health Monit. 18 (2011) 554-573

[11] Mohinder S. Grewal, Angus P. Andrews, Kalman Filtering: Theory and Practice Using Matlab, John Wiley & Sons, Inc.

[12] Anil K. Chopra-Dynamics of structures-Prentice Hall (2006)

[13] EN 1993-1-9 (2005) (English): Eurocode 3: Design of steel structures - Part 1-9: Fatigue [Authority: The European Union Per Regulation 305/2011, Directive 98/34/EC, Directive 2004/18/EC]